

Short-Term Orbital Forcing: A Quasi-Review and a Reappraisal of Realistic Boundary Conditions for Climate Modeling

Rodolfo G. Cionco^{a,*}, Willie W.-H Soon^b

^a*Comisión de Investigaciones Científicas de la Provincia de Buenos Aires – Universidad Tecnológica Nacional, Colón 332, San Nicolás (2900), Bs.As., Argentina*

^b*Harvard-Smithsonian Center for Astrophysics, Cambridge, Massachusetts, 02138, USA*

Abstract

The aim of this paper is to provide geoscientists with the most accurate set of the Earth's astro-climatic parameters and daily insolation quantities, able to describe the Short-Term Orbital Forcing (STOF) as represented by the ever-changing incoming solar radiation. We provide an updated review and a pragmatic tool/database using the latest astronomical models and orbital ephemeris, for the entire Holocene and 1 kyr into the future. Our results are compared with the most important database produced for studying long-term orbital forcing showing no systematic discrepancies over the full thirteen thousand years period studied. Our detailed analysis of the periods present in STOF, as perturbed by Solar System bodies, yields a very rich dynamical modulation on annual-to-decadal timescales when compared to previous results. In addition, we addressed, for the first time, the error committed considering daily insolation as a continuous function of orbital longitudes

*Corresponding author

Email addresses: gcionco@frsn.utn.edu.ar (Rodolfo G. Cionco),
wsoon@cfa.harvard.edu (Willie W.-H Soon)

with respect to the nominal values, i.e., calculating the corresponding daily insolation with orbital longitudes tabulated *at noon*. We found important relative differences up to $\pm 5\%$, which correspond to errors of 2.5 W m^{-2} in the daily mean insolation, for exactly the same calendar day and set of astro-climatic parameters. This previously unrecognized error could have a significant impact in both the initial and boundary conditions for any climate modeling experiment.

Keywords: Astrometry and Geosciences, Orbital forcing, Solar irradiance, Short-term perturbations

1. Boundary conditions for climate system: A brief historical review of orbital modulations of incoming solar radiation

The historical development for a scientific understanding of weather and climate change, particularly the astronomical theory of climate change is a long one (Neumann, 1985). For example, the Roman writer on agriculture, Lucius Columella (ca. 4 to 70 AD) began in his Book I De Re Rustica [On Agriculture]:

“For I have found that many authorities now worthy of remembrance were convinced that with the long wasting of the ages, weather and climate undergo a change; and that among them the most learned professional astronomer, Hipparchus, has put it on record that the time will come when the poles will change position, a statement to which Saserna, [or Sasernas because J. Neumann noted that this is most likely the writing from a father and son team] no mean authority on husbandry, seems to have given credence. For in that book on agriculture which he has left behind he concludes that the position

of the heavens had changed from this evidence: that regions which formerly, because of the unremitting severity of winter, could not safeguard any shoot of the vine or the olive planted in them, now that the earlier coldness has abated and the weather is becoming more clement, produce olive harvests and the vintages of Bacchus in the greatest abundance. But whether this theory be true or false, we must leave it to the writings on astronomy.”¹

Fast-forward to modern scientific age, the well-known calls for “weather forecasting as a problem in physics” and “climate as a problem of physics” (c.f., Monin and Shishkov, 2000) as well as the recent quest for “a theory of climate” (Essex, 2011) clearly exemplify and highlight the struggle of the science of meteorology and climatology for the past century till today. We may echo the most pristine quest set out by one M. Milanković, among other accomplishments also conferred as the father of climate modeling by Berger (2012) upon a comprehensive review of the subject, that:

“... such a theory would enable us to go beyond the range of direct observations, not only in space, but also in time... It would allow reconstruction of the Earth’s climate, and also its predictions, as well as give us the first reliable data about the climate conditions on other planets.”²

Such facts and reality alone would demand an ever increasing scrutiny for

¹The full text of this book is available at http://penelope.uchicago.edu/Thayer/E/Roman/Texts/Columella/de_Re_Rustica/1*.html.

²From p. 6 of Petrović (2009) where the first sentence of the quote has original words taken directly from Milanković’s autobiography. We wish to note that the Wikipedia entry for Milutin Milanković https://es.wikipedia.org/wiki/Milutin_Milankovi%C4%87 has incorrectly implied the quote to be from a 1913 paper entitled “Distribution of the Sun radiation on the Earth’s surface” (in Serbian).

a better precision and accuracy in defining and specifying what has been well accepted to be the so-called external forcing boundary conditions for Earth's complex and coupled climate system which involves not only the atmosphere, land and ocean per se but must also necessarily includes a host of other fast, slow and intermediate scales processes involving both the intrinsic magnetic variations and modulation of the Sun's radiation outputs and the distinct effects from gravitational interactions of all bodies in the Solar System (SS) in affecting the geometrical variations of the Moon-Earth's orbital elements. This basic requirement for a correct boundary condition for climate modeling can be sharpened further if climate variations are considered as a characteristic to be deduced from rather than artificially imposed on a realistic climate model (e.g., Nicolis and Nicolis, 1995; Lions et al., 1997; Goody, 2007).

It is clear from a careful literature review (see detailed discussion below for a brief review of those longer term orbital changes) that the limited availability of STOF parameters has thus far prevented from a more direct prescription of this particular boundary condition in any meteorological and climatic simulations and studies of the past, present and future. To the best of our knowledge, a rare exception is contained in the preliminary study by Bertrand et al. (2002). A close inspection from the United Nations Fifth Assessment Report (see Collins et al., 2013, p. 1051) tells us that STOF is indirectly assumed to be unimportant and play no climatic role. The primary argument and assumption in neglecting changes in orbital forcing for climatic changes over the last few thousand years, last century or even last decade seemed to be from the claim that *globally-averaged* radiative forcing is small or negligible. Other reasoning, involved in climate reanalysis projects

and products (see e.g., Simmons et al., 2014; Hersbach et al., 2015), seemed to be that such an effect involved in the modulations of the seasonal forcing and seasonality itself has been indirectly included in other boundary conditions like through the prescription of sea surface temperatures or atmospheric ozone concentration or through assimilation of other atmospheric metrics in a 100-year atmospheric reanalysis simulation.

More than two decades ago, (Laskar et al., 1993, p. 525) echoed a reminder that:

“The mean annual insolation depends thus only on the eccentricity of the Earth, and its variation over 1 Myr are . . . [very small, about 0.6 W m^{-2} as shown in Figure 4 of Laskar et al. 1993] . . . In fact, this is not the main paleoclimate quantity, and it was recognized by [Milanković] . . . that the summer insolation at high latitudes had a larger influence on the climate of the past. If the insolation in summer is not high enough the ice does not melt, and the ice caps can extend. This is why it is also important to compute the daily insolation at a given point on the Earth.”

We agree and only wish to call for a more direct accounting for STOF, as a true boundary condition, in all climatic simulations in that the effects from local and regional perspective are clearly not negligible nor unimportant (see e.g., section 3.7 in Miller et al., 2014) in terms of seasonal dynamical evolution of the coupled air-sea-land system. The importance of accurately specifying the incoming solar radiation on local and regional geographic scales should also be studied and assessed in contexts with the currently unresolved difficulties in closing the budget of Earth’s energy imbalance (Trenberth et al., 2016) as well as in both interpreting and emulating local and regional surface

temperatures using the state-of-the-art general circulation models (Ji et al., 2014; Lin and Huybers, 2016). Furthermore, the persistent modulation of the orbital forcing, via the modulation of the seasonal irradiation amplitudes, ranges and their geographical distributions, all across the globe may yield a deeper insight to the basic problems of climate science on timescales of decade to century.

We shall limit our exploration and calculation to the Holocene and 1 kyr into the future, for which the longest available accurate ephemeris including this period is the Jet Propulsion Laboratory’s Development Ephemeris 431 (JPL’s DE431) outputs (Folkner et al., 2014). Another simplification we adopt for this paper is the postponement of the accounting of the intrinsic variations of the Sun’s irradiance outputs as caused by the variable nature of solar magnetism on a host of timescales but a recent review on the choices of Total Solar Irradiance (TSI) records to use for climatic study and modeling has been reported in Soon et al. (2015).

We will not further speculate on the importance of getting the correct boundary conditions for any atmospheric, meteorological and climatic simulations, but will limit ourselves to a brief note on some recent works as a source of motivation. Cronin (2014) has recently highlighted the key role of getting the solar zenith angle correctly represented in global climate models where errors in assuming daytime-average zenith angle or spatially constant insolation may lead to underestimating or overestimating of global energy budget on the order of 10 W m^{-2} or more, respectively. Hogan and Hirahara (2016) documented the situations when the infrequent calls to radiation module in a climate model calculation may lead to errors in stratospheric tem-

peratures of 3 to 5 K. He et al. (2015) spelled out the detailed dependence of the amount of solar radiation on the length of day and latitude which in turn for defining the role of Tibetan and Iranian Plateau in constraining the northerly intrusion into the Indian monsoon area during boreal summers. The multi-scale roles of solar radiation on the diurnal cycles and related coupled ocean-atmosphere dynamics of the warm surface ocean including tropical Indian Ocean and the western equatorial Pacific have been examined by Shinoda (2005) and Li et al. (2013). Hudson et al. (2016) highlighted the key role by solar irradiation impacts for the reflection heights in the ionosphere that are changing by 15 km, 12 km and 1 km, respectively, by diurnal, seasonal and 11-yr cycles of solar irradiation. Jajcay et al. (2016) shows and discusses the evidence on how the small-amplitude 7-8 yr oscillations in the European surface air temperature records can produce the so-called cross-scale modulation in the temperature at a higher frequency range and regime, in their case the annual cycles. It is far from clear that the multi-scale STOF reality presented in our paper would have absolutely no role for this case study by Jajcay et al. (2016). Finally, Joussaume and Braconnot (1997) and Chen et al. (2011) have cautioned earlier on concerning the differences in calendar assumptions (i.e., differences in the Sun's positions with respect to calendar days) that can lead to a rather significant impact in climate modeling through phase shifts on the prescribed solar irradiance values. This is why, as emphasized in this work, an accurate and reliable way of tracking time in the orbital calculation is important.

2. A quasi-review and overview of several important previous works

From a paleo-climatic perspective, the most widely applied studies related to changes in the incoming solar radiation (the so called insolation) due to variations in both Earth’s orbit and Earth’s celestial pole, have been considered in detail by, e.g., Berger (1978) and references therein, Berger and Loutre (1991), Laskar et al. (2004, 2011a) for a very long time-span (i.e., geologic eras). Such long-term forcing, varying on tens to hundreds thousands of years on incoming solar radiation, is often called the *Milanković orbital forcing*. These works are effort based on celestial mechanics publications of Milanković (1941), Sharaf and Boudnikova (1967), Bretagnon (1974), Berger (1978), Laskar (1988), and Laskar et al. (2004) among others. Both Imbrie (1982) and Berger (2012) proffered a comprehensive review on the history of the *orbital solutions* which now have improved techniques and methodologies starting with the classical orbital problem of the evolution of the gravitational solar N -body system, which have their roots in the works of Laplace and Lagrange (see e.g., Laskar, 2013).

These solutions (as it is usually referred to in astronomical literature for the process in obtaining orbital elements and Earth’s orientation parameters from a semi-analytic model of the SS evolution) are intended for several million years. Such calculations are based on the numerical integration of the equations which describes the secular (i.e., long-term and long-period) dynamics of the SS, where short-term periodicities, arising from the evolution of the orbital longitudes itself, were simply not taken into account in order to reduce the complexity of the orbital integrations. Specially, the works by Berger and Loutre (1991) cover the field for -5 Myr (i.e., before

present); Laskar et al. (2004) integrate a secular-realistic model of the SS, given accurate solutions for -50 Myr and $+20$ Myr from present. Laskar et al. (2011a) also using very accurate initial conditions and very short time step (less than one year), have recently extended the previous solution to -250 Myr, i.e., including all the Cenozoic era.³ These solutions coming from works by Laskar and colleagues although permitting the *insolation quantities* at, e.g., annual timescale, but all those impressive results did not account for the STOF variations.

The key issue tackled in our present work is the problem of the short-term variations of insolation quantities; i.e., the high-frequency orbital forcing, and its variations at decadal and multidecadal scales. This problem was first addressed by Borisenkov et al. (1983) and Borisenkov et al. (1985). They determined short timescale variations between ~ 2 -20 yr which produce variations of the same order as the long-term orbital forcing in a few hundred years. They found that the greatest short-term effect of orbital forcing occurs in high latitudes at midsummer (July); with the lunar orbital retro-grading period of 18.6 yr (i.e., the main nutation term) as the most evident driver (see e.g., the recent evidence found for this modulation of sea level at the Eastern North Sea and Central Baltic Sea regions by Hansen et al., 2015).

³In addition to what was already known about the chaotic evolution of orbital motions of terrestrial planets in the SS with a characteristic Lyapunov time of 5 Myr (i.e., largely limited by the lack of knowledge on the precise value of solar oblateness, J_2), it is worth noting that Laskar et al. (2011b) recently proposed that “it will never be possible” to track the precise evolution of the Earth’s eccentricity beyond 60 Myr owing to the strong chaos caused by close encounters or even a chance collision between Ceres and Vesta.

This effect is found to be of the same order of amplitude as the intrinsic irradiance variations due to solar magnetic cycle variations. Loutre et al. (1992) performed the most complete analysis of short-term orbital forcing to date. They analyzed the Earth's parameters involved in orbital forcing, which are the so-called *astro-climatic elements* or parameters, for the last 6 kyr at an annual basis (i.e., getting one value for each calendar year). Their astronomical solution is based on the French VSOP planetary theory (Bretagnon, 1982). This semi-analytic theory, was developed in series up to third order of the masses of all the planets considered plus an improvement for the descriptions of the giant planets up to the sixth order. The lunar perturbation in the Earth-Moon barycenter is also included; but the Earth and the Moon are not considered as separated bodies. The basic integration constants used were adjusted from former JPL DE200 ephemeris (Standish, 1982). Therefore, this solution allowed considerably shorter periodicities in planetary perturbations than former astronomical solutions. Loutre et al. (1992) confirmed the earlier results of Borisenkov and collaborators, showing that the most important spectral peaks occur at decadal timescales (say, periods less than 40 yr), but also specified longer periodicities, some of them at multicentennial to nearly millennial scales. They found that, for longer periodicities the precessional modulation produced the most important signals for low to middle latitudes, with the obliquity signals stronger at solstices for polar latitudes. Such an observation is clearly consistent with what is mostly known for the Milanković orbital timescales (see e.g., Imbrie, 1982).

It would be premature for us to spell out and prove the direct relevance of all such STOF periodicities for any ranges of climatic measures and metrics

while the state of understanding and discussion in the literature remains still largely unsettled. This is mainly because there has been little, with the few exceptions reviewed here, study for STOF in terms of any actual manifestations in the real external boundary conditions that can be subjected to any systematic evaluations.

Although Milanković forcing data are available (Berger and Loutre, 1991; Laskar et al., 2004, 2011a), e.g., from the National Centers for Environmental Information of NOAA/NCEI [formerly known as NOAA/NCDC] (<http://www.ncdc.noaa.gov/data-access/paleoclimatology-data/data-sets/climate-forcing>),

detailed STOF data and the corresponding insolation quantities are still largely missing from any scientific archives and literature. Secular (smooth) values of insolation quantities can be obtained at centennial resolution using orbital solutions by Laskar and colleagues, from this web page (but, as was mentioned, only strictly for Milanković's scales of oscillations in tens of millennia). To-date, there is no direct data made available publicly, e.g., from Loutre et al. (1992) solution, describing STOF and insolation quantities. Hence, we have decided to provide geoscientists with the most complete and accurate descriptions of the STOF astro-climatic parameters using DE431 ephemeris, the longest high precision ephemeris publicly available. High precision ephemerides have the most accurate description of short-term variations of Earth's orbit. Another important improvement (i.e., with respect to Loutre et al. 1992) worth applying now is the use of the latest precession-nutation formulas to get the astro-climatic parameters expressed in a reference system of *the date* (i.e., with respect to the moving equinox).

Although a large effect may not be expected in our studied time-span of the Holocene, it is important to use these latest formulations if an accurate accounting of the dynamics of orbital forcing is desired. The classical polynomial precession formulas (Lieske et al., 1977) are only valid for a few centuries from J2000.0 (Vondrák et al., 2011) and non-rigid Earth nutation series are now available (Mathews et al., 2002) for our inclusion.

From Milanković works to present, the incoming solar radiation has been reckoned in different ways (i.e., the so called insolation quantities: instantaneous, daily, mean mid-month, monthly mean, seasonal, etc.). We think that any arbitrary uses of insolation or derived quantities related to it, could be confusing to expert modelers and non-expert readers alike. The basic insolation definitions and calculations over arbitrary period of times are periodically reviewed and explained in terms of the most basic geometry or refined mathematical tools (e.g., Berger, 1978; Laskar et al., 1993; Berger et al., 2010). In this work we also feel that it is necessary to start reviewing the basic definition of insolation. They are based on daily irradiation over a whole Earth's variable rotation day (Berger, 1978; Berger et al., 2010; Borisenkov et al., 1985; Loutre et al., 1992) which is the basis or foundation of all longer time-span calculations.

Daily irradiation is the fundamental parameter of all insolation calculations and its formulation is derived considering the constancy; over a full day, of astro-climatic elements and also the solar orbital longitude (therefore, the solar declination; see Section 3), assuming that the error committed considering this constancy of orbital longitude is also negligible (Berger et al., 2010). Nevertheless, for practical purposes, daily insolation formulas are usually ap-

plied, considering the metric as a *continuous function of solar longitude*; i.e., as a continuous function of time, setting a desired longitude value, which, in fact, could be anything within a particular day. Such a procedure in adopting the daily insolation formulas as a continuous function of solar longitude, is an habitual practice in paleoclimates studies, where insolation variations at a particular orbital longitude (e.g., solstices, equinoxes, etc.) is followed along the ages. The error with respect to the nominal (i.e., a constant solar longitude) daily insolation formulas has not been addressed in the literature, although one can assume a level of accuracy of 0.01 W m^{-2} in the mean daily insolation, following the claim in Berger et al. (2010). In this work, we have tabulated accurate daily insolation quantities at periods of one day (one Julian day of 86400 s); so we can evaluate the difference or “error” in evaluating the same insolation quantities, adopting both approaches, calculating daily insolation formulas as a continuous function of orbital longitude and using tabulated values at noon of the corresponding day.

The main aim of this work is to describe and calculate the short-term dynamics of the Earth’s astro-climatic elements, with the highest precision available and the basic daily insolation quantities suitable for climatic modeling, for the whole Holocene up to 1 kyr in the future. We present our analyses adopting the solar true orbital longitude coordinate in order to avoid “calendar-problems” related to “fixed-day” calendar used in most paleoclimate studies (Joussaume and Braconnot, 1997; Chen et al., 2011; Steel, 2013). Nevertheless, we also express our data in Julian days; which is a standard time-reckoning in astronomy, this also provides a link to civil calendar of the past and future. Although STOF variations produce departures of the

secular, long-term values less than $\pm 0.15 \text{ W m}^{-2}$, we found that calculating daily insolation quantities with tabulated values for a certain day or using it as a continuous function of orbital longitude, can produce important differences, up to $\pm 2.5 \text{ W m}^{-2}$ ($\pm 5\%$) in the mean daily insolation, for the same set of astro-climatic parameters. This holds even for the present day. Again, along our theme of climatic variations should be a *deduced* characteristics of the Earth’s coupled non-linear dynamical system, we consider that taking additional cares in accounting for this aspect of STOF boundary conditions in any climate simulation or attribution studies are both necessary and important.

3. Solar irradiance intercepted (or received) by the Earth and co-ordinate systems for studying STOF variations

Let us define the instantaneous solar irradiance received at the top of the atmosphere above a geographic location on Earth, at a certain moment of a given date. The amount of solar energy flux, Q_t , on a horizontal surface per unit of time, depends on the received Total Solar Irradiance, TSI, (i.e., the total energy received from the Sun) which, as a flux, depends on the inverse-squared-law to the source, for us the Sun-Earth distance r (reckoned in astronomical units, au), and on the inclination of sun beams as follows:

$$\frac{dQ_t}{dt} = I = \text{TSI}(r) \cos z; \quad \text{TSI}(r) = \text{TSI}_0 \left(\frac{1\text{au}}{r} \right)^2, \quad (1)$$

I is the instantaneous received solar irradiance, the intensity of the vertical component of sunshine, or the incoming solar radiation (insolation); in MKS system the insolation is reckoned in $\text{J}/(\text{s m}^{-2})$ or W m^{-2} . TSI_0 is the “solar

constant”, the solar irradiance received at a fiducial distance by a surface directly oriented to the Sun. The angle subtended by the Sun from the zenith, i.e., the zenithal distance, z , can be expressed as functions of the latitude of the observer and of the declination of the Sun, δ , as shown in Fig. 1. Here a local fixed geocentric equatorial system (X,Y, Z) is defined, X directed towards the local meridian; $-Z$ towards the hemispheric pole (south, here); therefore the direction of the Sun, \check{n}_{\odot} , and the direction of the observer’s zenith, \check{n}_z , can be written as:

$$\check{n}_{\odot} = (\cos \delta \cos H, \cos \delta \sin H, \sin \delta); \quad \check{n}_z = (\cos \phi, 0, \sin \phi), \quad (2)$$

where H is the hour angle (reckoned from the local meridian, following the sense of the Sun’s apparent motion). To avoid confusion with sign conventions, we assume that δ and ϕ are the absolute value of the celestial and terrestrial angles to depict the problem and to consider in our formulation; in subsequent applications we must put the corresponding signs (in fact in Fig. 1, δ and ϕ need to be negative numbers to fulfill the right-hand rule of the coordinate axes). Besides, we neglect the diurnal parallax effects, so the geocentric angles are equal to topocentric ones (this assumption leads to a correction at a maximum of 9 arcsec). It is thus straightforward that:

$$\cos z = \check{n}_z \cdot \check{n}_{\odot} = \sin \phi \sin \delta + \cos \phi \cos \delta \cos H, \quad (3)$$

then we can write the flux of the solar energy projected on a horizontal plane, per units of time as:

$$\frac{dQ_t}{dt} = I = \text{TSI}_0 \left(\frac{1\text{au}}{r} \right)^2 (\sin \phi \sin \delta + \cos \phi \cos \delta \cos H). \quad (4)$$

As a note, the “solar constant” for us is the index received at 1 au (a fix distance to the Sun), e.g., $1364.5 \pm 1.38 \text{ W m}^{-2}$ (Mekaoui et al., 2010); but an estimation based on the mean Sun-Earth distance: $\langle r \rangle = a\sqrt{(1 - e^2)}$, where a is the Earth’s orbit semi-major axis and e the Earth orbital eccentricity; produces a different factor of $(1 - e^2)^{0.25}$ in Eq. (4). The importance of getting the absolute value of TSI_0 index correctly for climatology has been recently discussed and explored in Soon (2014). For all the calculations in this paper, we adopted $\text{TSI}_0 = 1366 \text{ W m}^{-2}$ mainly to provide an apple-to-apple comparison with the numerical results shown in Loutre et al. (1992) but of course TSI_0 is left as an adjustable free parameter in our computer programs.

It is evident that for a fixed latitude, the insolation I depends strongly on seasonal changes which are driven by annual solar declination variations, with the Earth-Sun distance virtually constant at intra-annual timescale, with respect to δ variations. This can be clearly seen by relating r and δ with the Earth’s astro-climatic parameters (Berger and Loutre, 1991; Loutre et al., 1992); the above mentioned eccentricity, e ; the longitude of the perihelion, ϖ ; and the obliquity of the ecliptic (Earth’s obliquity), ϵ :

$$r = \frac{a(1 - e^2)}{1 + e \cos(\lambda - \varpi)}; \quad \sin \delta = \sin(\lambda + 180^\circ) \sin \epsilon \quad (5)$$

where λ is the true longitude of the Earth on its orbit, a polar angle of position of the Earth reckoned from the equinox of reference (γ_0) which sets the reference system on which these elements were originally depicted and calculated (see Fig. 2). In what follows, we consider the Earth’s semi-major axis to be a non-constant parameter, because it has short-term variations

(but not secularly growing, at least, under the considered Holocene interval of twelve to thirteen thousand years), hence this parameter will produce a slight variation on the solar radiation received (of course, if we assume solar constant evaluated at $r = a$; then a disappears in the formulation).

In paleoclimate studies, it is usual to set the Sun's longitude, which we have already emphasized, and is defined as $\lambda_{\odot} = \lambda + 180$, and not the Earth's longitude, because the apparent geocentric solar movement is described. Hence, in order to identify the correct time of the year when solstices and equinoxes occur, i.e., when the Sun passes through them in its geocentric orbit, we have indicated in Fig. 2, the month of the year (for the present calendar time) and the corresponding position of the Sun in its reflex orbit. Here, the vernal equinox (origin of longitudes) corresponds to $\lambda_{\odot} = 0$ deg. (March), the June solstice is at $\lambda_{\odot} = 90$ deg. (i.e., the Earth is near its aphelion), the equinox of September is at $\lambda_{\odot} = 180$ deg., and the solstice of December $\lambda_{\odot} = 270$ deg. (i.e., when the Earth is near its perihelion).

At this point, it is important to remember that day by day, the origin of orbital longitudes, the γ point, makes a complex movement involving components of longer period (precession) and shorter period (nutations). Such movements are produced by the combined planetary and luni-solar torques which, in turn, affect the reckonings of longitude and also the Earth's obliquity (see Fig. 2 and the next section); i.e., the Earth's pole positions on the celestial sphere.

Eq. (5) clearly shows that the movement of the origin of longitudes has a dramatic effect on the apparent positions of the Sun in the sky with respect to the seasons. Because of this, we need to keep the synchronization of the

orbital longitudes with the seasons. Therefore, the origin of longitudes needs to be measured from the “true –i.e, real and moving– equinox of the date” (γ); hence if we call λ_t the true longitude and ϖ_t the longitude of the perihelion of the Earth measured from the *true equinox of the date*, we must replace them in Eq. (5); then the trigonometric part of both equations become $\cos(\lambda_t - \varpi_t)$, and, $\sin(\lambda_{\odot t})$, with $\lambda_{\odot t}$ as the true solar longitude *of the date*. For the reference to calendar date (Gregorian, leap year mechanics), time is kept following the precession, i.e., it is set, as far it is possible, to tropical year, then the seasons are set with the months of the year at least for several thousand years before and after present. Nevertheless, inconmensurabilities between the involved periodicities and proper irregularities of the changing Earth orbital elements, produces that fixed values of λ_t does not occurs exactly at the same calendar date. In other words, the duration of the season varies through time. In paleoclimate, a *conventional* calendar is used, it is the present Gregorian calendar, with the present month versus Earth’s longitude relationship. Nevertheless, for the above-mentioned reasons (fixed values of longitude do not occur exactly at the same date), important differences in insolation estimates can occur when calendar date is used as temporal reference, even with the conventional calendar (Joussaume and Braconnot, 1997; Steel, 2013, see below).

In what follows, we explain how to obtain high precision astro-climate elements from DE431 for the studied time span. Because we used a standard ephemeris, we obtain the basic data at a certain fix time step, based on a fixed Earth’s day of 86400 s, the Julian day. This is the standard way by which the SS bodies are positioned at a certain moment. It is interesting to

note that this will also provide an exact link to the civil (Gregorian – Julian) calendar.

4. Some astrometry

With the advent of fast computers, it is possible to resolve, by direct numerical integration, the set of differential equations which describe very accurate models of the planetary problem in the SS using high precision initial conditions, for a very long time span. Moreover, the integrated orbits can be fitted to observations which improves the final precision of the solution. In this way, we can get for instance, the heliocentric position, \mathbf{r} , and velocity, \mathbf{v} , of the Earth as a function of time; this process is referred to as the *ephemeris calculation*. DE431 ephemeris models the Earth’s center of mass movement in the SS and some parameters of Earth’s orientation in the inertial space. The position and velocity of the Earth are obtained by adopting the relativistic-barycentric reference system, related to the barycenter of the SS. Later, for a specific moment, through an *orbit calculation*, we can replace this set of six components of \mathbf{r} and \mathbf{v} with six “constants” of motion, the Keplerian elements, which have the convenient property for describing the orbital ellipses of the Earth around the Sun. Even more nicely, we can describe the apparent geocentric orbit of the Sun around the Earth with such a set of elements. Of course, through time, these “constants” vary because there are more than two bodies (some of them significantly non-spherical bodies) orbiting and interacting. Then, we need to follow through time the Earth’s orbital elements as well as the orientation of the Earth celestial pole in space. These variations are the geometrical causes of insolation variations.

As mentioned, the longest high precision ephemeris publicly available is the JPL’s DE431 integration (Folkner et al., 2014). It is designed to cover from 13,200 years before the reference epoch J2000.0 to 17,191 years after. And DE431 is in good agreement with all the main ephemerides, i.e., the French INPOP (Fienga et al., 2008) and the Russian EPM ephemeris (Pitjeva and Pitjev, 2014). Unlike semi-analytical planetary theories such as VSOP (Simon et al., 2013), numerically integrated ephemerides naturally include *all* the terms of the disturbing functions; and integrates separately the Earth, from the Earth-Moon barycenter so it provides the best description for short-term variations on decade to century.

4.1. Issues of time keeping in brief

The time used in the dynamical equations of the ephemeris model is reckoned in a relativistic (coordinate) timescale, expressed in TDB (time dynamical barycentric) units. This TDB time units evolves in a different scale with respect to the timescale in which our civil time (the time expressed in our watches) is based: the UTC (universal time coordinate). Our civil time, can be easily related to true solar time, which describes the Sun’s position with respect to the observer’s meridian at certain moment for a date. But UTC is not a dynamical timescale (i.e., UTC is not a relativistic-coordinate time). The corresponding coordinate time for an Earth observer is TT (terrestrial time). Fortunately, the difference TDB–TT is less than 2 ms for several millennia (see e.g., Kaplan, 2006). So we can presumed TT to be equivalent to TDB (and vice versa) as a temporal reference related to orbital elements and all derived quantities from them. Therefore, we can assume that one can accurately represent the Earth’s orbital elements in

TT timescale. For example, a solar longitude recorded in DE431 at fiducial J2000.0 epoch, corresponds to Julian day JD 2451545.0 (TT), or the calendar date 1/1/2000, 12 h TT, which is equivalent to 1/1/2000 11:58:55.816 UTC; i.e., at the approximate noon of an observer at Greenwich.

The relationship of UTC with TT has its own problems. UTC is based on atomic international time, which has a uniform scale, but UTC is subjected to leap second corrections. The corrections were done in order to keep UTC nearest to the rotational time; which is in turn non-regular because of the Earth's irregular rotation. The effect of the variability in Earth's rotation has a clear documented evidence in the past and it has a fundamental role on daily insolation determination, because the solar day depends on Earth's rotation. Through this leap second correction, UTC is closely related to the universal time (UT). This timescale has all the irregularities of Earth's rotation. UT is studied and adjusted using ancient astronomical observations and following Morrison and Stephenson (2004) for the interval 9999 BC-700 BC, the difference TT-UT (which, for our purposes we can assume as TDB-UT) follows a parabolic relationship such that for BC10000 = 1/1/-9999 = JD-1931076.0 (TT), we have TT-UT = 5.17 h, which is often referred to as the "clock error". This difference shows us that a certain phenomenon (e.g., the Sun's position at noon) reckoned in TDB relativistic-uniform timescale, has probably an uncertainty of that amount when we try to refer as a geocentric phenomenon to be observed at that epoch. This also implies that the present nominal 86400 s for the length of the day (LOD) is no longer valid for ancient ages. This clock error is not usually mentioned nor discussed in paleoclimatic studies, but it is important to take into account

for detailed modeling into the past. Therefore, the daily solar irradiance that has been extensively used (Berger, 1988; Berger et al., 2010), based on LOD of 86400 s, produces a very different estimation of the “real” daily insolation received in a whole true solar day of a certain remote epoch in the past (or future). Regarding civil calendars, it is important to remember that calendar days refer to the Julian calendar dates before 4th October 1582. Julian calendar has its own reckoning of the year duration; then, the JD for some events in the past (as solstices or equinoxes) has an offset of several calendar months with respect to the present calendar.

4.2. Obtaining Earth’s orbital elements from DE431

The JPL website (<ftp://ssd.jpl.nasa.gov/pub/eph/planets/Linux/de431>) provides a binary file of DE431 ephemeris, tailored for Lynux users, the `lnxm13000p1700.b` file; the temporal limits of this file are 9/12/-13001 and 11/1/17000. As far as we know there is no simple program (e.g., FORTRAN code) to read and directly obtain \mathbf{r} and \mathbf{v} from it. But JPL provides a Fortran code for testing another version of ephemeris in binary blocks, `THESTEP.f` routine. We have modified this routine to get Earth’s \mathbf{r} and \mathbf{v} with full precision for an arbitrary time step. Then, we performed an orbital calculation with a time step at every one Julian day. Thus, we are getting astro-climatic elements at each day which is a huge improvement over other estimates which considered only annual-resolution settings (e.g., Loutre et al., 1992). In this way we obtain a full set of Earth’s orbital elements and positional angles: the semi-major axis, eccentricity, inclination, longitude of the perihelion, longitude of the ascending node, mean anomaly, true longitude and the true anomaly all with respect to the reference epoch J2000.0, in

TDB \simeq TT timescale. Therefore, for present times or instances, assuming a constant Earth rotation speed (86400 s), an observer at Greenwich meridian has such a precise set of Earth’s elements and solar longitudes, at noon, to calculate insolation quantities.

In what follows, and mainly to represent quantities as function of the time, when we make mention of “time in years”, for a specific Julian day number J , we refer to Julian epoch:

$$t = 2000.0 + \frac{J - 2451545.0}{365.25}, \quad (6)$$

which enable us to reckon the variable time, t , as a real number (i.e., in years and the fraction of a year).

The orbital calculation only determines ϖ and λ measured from the fixed fiducial (γ_0) J2000.0 mean equinox and ecliptic. However, in order to obtain these quantities but measured with respect to the true equinox of the corresponding date, we must deal with the long-term and short-term motions of both the equator and the ecliptic.

5. The motion of basic planes

Luni-solar and planetary torques modify the Earth’s celestial pole and the pole of the ecliptic, which are described by the combined actions of the longer term (i.e., longer than 100 centuries) precessional as well as the shorter nutational changes. Mean precessional changes describe the evolution of the mean equator and ecliptic at a certain date. In our STOF calculation, we want to take into account the shortest variations of these planes; i.e., we need to describe both the *true* ecliptic and equator of the date. The eclip-

tic is defined as the mean plane of the Earth-Moon barycenter orbit around the SS barycenter (i.e., perpendicular to the Earth-Moon orbital angular momentum vector with respect to the SS barycenter). Both, the ecliptic and equatorial planes, are subjected to luni-solar and planetary perturbations (Vondrák et al., 2011; Capitaine and Soffel, 2015). Fig. 3 shows the precessional elements with respect to the J2000.0 reference epoch. The accumulated precession (subscript A) of the equator with respect to the reference epoch is described by ψ_A and ω_A (in longitude and obliquity, respectively); the corresponding elements of the ecliptic precession are Π_A and π_A . The mean obliquity of the date (i.e., only affected by precession) is ϵ_A . Then, the *general precession in longitude* accumulated from J2000.0 is:

$$p_A = \Lambda_A - \Pi_A, \quad (7)$$

an arc of great circle describing the absolute motion of the mean γ point along the ecliptic of date; it combines the precession in longitude of equator and the precession of ecliptic. To represent the long-term variations of these elements we used the model provided in Vondrák et al. (2011), which is a significant improvement with respect to the model described in Loutre et al. (1992) that was in turn based on the older IAU standard of Lieske et al. (1977). Vondrák et al. (2011)'s parametrization is based on numerical representations of mean equator and ecliptic (e.g., Laskar et al., 1993), which are consistent with the JPL's Development Ephemeris.

5.1. Combining secular and short-term variations for new astro-climatic elements

The elements coming from DE431 define and orient the plane of the Earth’s orbit of the date with respect to the reference epoch (J2000.0). Recall the fact that DE431 separates the Earth from the Moon, therefore we can describe the “true” Earth’s orbit around the Sun. Then, for our astro-climatic short-term solution, we need to combine the long-term/short-term variations represented by precessional-nutational parameters and those specific Earth’s orbital orientation elements which contain both secular and short-term variations that in turn were derived from the DE431 ephemeris. This particular geometry is described and summarized in Fig. 4. Although DE431 uses an improved precession model for the orientation of Earth; which is a rigorous numerical integration of the equations of motion of the celestial pole using Kinoshita’s solid Earth model (Kinoshita, 1977) for the speed of luni-solar precession (Owen, 1990), which, however, is not the actual Vondrák et al. (2011)’s model. We think that such a mismatch is not a big drawback because the impact of Earth’s true orientation on Earth’s center of mass integration should be small for the Holocene time-span we considered in this paper. We contacted Dr William Folkner of NASA JPL and he strongly recommended using Vondrák et al. (2011) precession formulas as the detailed model for the long-term evolution of Earth’s orientation to couple jointly to the DE431 ephemeris.

In Fig. 4, we replace the ecliptic of the day with the Earth’s orbital plane, defined through DE431, so we approximate:

$$\pi_A = i; \quad \Pi_A = \Omega, \quad (8)$$

where i is the *inclination* of the Earth’s orbit in the fiducial reference system; Ω is the ascending node. In addition, we add the nutation in longitude and obliquity to the equator movement, therefore:

$$\psi_t = \psi_A + \Delta\psi_A; \quad \omega_t = \omega_A + \Delta\omega_A, \quad (9)$$

where ψ_A and ω_a are obtained from Vondrák et al. (2011)’s theory. The $\Delta\psi_A$ and $\Delta\omega_A$ angles are the nutation in longitude and obliquity. The IAU nutation model, based on the 1980 IAU theory, is now being replaced with the new model of Mathews et al. (2002). Fortunately, its computational implementation is provided in the Standards of Fundamental Astronomy (IAU SOFA Board, 2016) through the SOFA software. We used IAU2000A model, which is the most complete version that includes all planetary and luni-solar effects on a non-rigid Earth with multiple couplings (see Mathews et al., 2002).

At this juncture, it is important to note that the arc describing the moving equinox (γ) over the orbital plane of the Earth is p_t . We could call p_t “the true general precession of the date” because it is the general precession affected by nutation and also by the approximate Earth’s orbit as specified from DE431 ephemeris. Therefore, the arc $N\gamma$ is now $p_t + \Omega$ in this new description (see Fig. 4). Hence, the changes in orbital longitude and in the longitude of the perihelion, described in Section (3), should be written as:

$$\varpi_t = \varpi + p_t; \quad \lambda_t = \lambda + p_t, \quad (10)$$

and this is equivalent to a change in the origin of longitudes from γ_0 to γ in Fig. 2. Also the obliquity in Eq. (5), must be replaced with the “true obliquity of the date”, ϵ_t . This permits us to find a new astro-climatic solution that we called the DE431-IAU solution.

6. New STOF astro-climatic elements: DE431-IAU solution

Now, we must find p_t and ϵ_t values as a function of time to obtain the true longitudes and obliquity of the date. Consequently, we need to solve the spherical triangle of Fig. 4, for which we follow a similar procedure as in Loutre et al. (1992). Using cosine formula (by angle):

$$\cos \epsilon_t = \cos \omega_t \cos i - \sin \omega_t \sin i \cos(\psi_t + \Omega) \quad (11)$$

and sine formula:

$$\sin(p_t + \Omega) \sin \epsilon_t = \sin \omega_t \sin(\psi_t + \Omega) \quad (12)$$

and five elements formula (2 sides, 3 angles; see e.g., Duriez, 2002):

$$\cos(p_t + \Omega) \sin \epsilon_t = \cos \omega_t \sin i + \sin \omega_t \cos i \cos(\psi_t + \Omega) \quad (13)$$

we get:

$$\tan(p_t + \Omega) = \frac{\sin \omega_t \sin(\psi_t + \Omega)}{\cos \omega_t \sin i + \sin \omega_t \cos i \cos(\psi_t + \Omega)}. \quad (14)$$

We wish to note a typographical error in Loutre et al. (1992)’s Eq. (12): the second member on the right hand side should be “+”. By solving Eqs. (11) and (14) we find a new set of astro-climatic parameters.

As a matter of consistency, we compare our results (p_t and ϵ_t); but removing the effects of nutation correction, with the corresponding long-term precessional elements of Vondrák et al. (2011), p_A and ϵ_A . The differences are smaller than 30 arcsec in obliquity and smaller than 60 arcsec in longitude for the whole 13 kyr interval studied; which produce a very small change in the solar radiation received, of $\sim 2 \times 10^{-4} \text{ W m}^{-2}$ at a maximum. Such a difference is significantly smaller than the nominal error committed in the theoretical calculation of daily irradiance (see next section). Therefore, we argue that both DE431 elements and IAU related precession+nutation models are sufficiently consistent and accurate for our purposes.

We show the full set of DE431-IAU astro-climatic elements (including *climatic precession*, $e \sin \varpi$) over the full time interval in Figs. 5, 6, 7 and 8, where one point for every 120-day has been plotted to avoid over-sampling effects. We wish to note that these sampling effects can produce the apparent spurious spikes in the representation of these elements, when you select these data at a greater time step. Indeed, the smallest periodicities involved in these orbital elements are of the order of a few months. The orbital periods of Mercury and Venus, which produce detectable spectral peaks in e.g., eccentricity, are about 0.24 yr and 0.6 yr, respectively (see also next section). At first sight, and comparing with Loutre et al. (1992) solution, the DE431-IAU solution seems to be “richer”, with the evidence being most obvious using the finest time resolution. The spectral analyses performed on them confirm our claim.

6.1. Short-term periodicities detected

We have explored spectral analyses on the DE431-IAU solution by using several methods; mainly, Lomb periodogram, maximum entropy and multi-taper method (MTM), and have found a profuse amount of spectral lines which basically include all the periodicities found in previous works. Short-term periodicities in astro-climatic elements were reported by Borisenkov et al. (1983) studying daily insolation variations at several latitudes; they were: 2.7 yr, 4.0 yr, 5.9 yr, 11.9 and 18.6 yr. Loutre et al. (1992) determined several short-term periodicities by analyzing first the variations of the astro-climatic elements. For daily insolation at 65°N, they found essentially the same periodicities (showing that the most important spectral peaks occur at decadal, say < 40 yr, time-scale), plus 8.1 yr, 15.7 yr and 29 yr periods; arguing that these last were coming from perturbations by Venus, Mars and Saturn. These are the main periodicities detected, but longer term periodicities (e.g., $\sim 40, 60, 800, 900$ yr) were also detected, but needing more detailed scrutiny and careful examination. We agree with Loutre et al. (1992) that MTM is a good choice for analyzing astro-climatic elements because this method produces less noisy spectrum with an easy way to calculate confidence levels; in this regard, we have used SSA-MTM toolkit from Ghil et al. (2002). Our results show strong non-linear trends in the spectra (which is clear from the element's graphics, Fig. 5-8), even while analyzing shorter portions of the time series; therefore, our analysis include a prior detrending of the time series. This is essential for a proper determination of the spectral peaks corresponding to the longer periods.

In astro-climatic elements, these short periodicities are associated with

planetary mean motions or combinations of them because the Earth’s disturbing function depends on these orbital configurations (see Roy, 1978; Murray and Dermott, 1999). These are generically called *inequalities* because the mean motion relationships $p n_i - q n_o$, where p and q are integers and n_i, n_o are the *mean motion* of both planets, oscillates around a small (say, few degrees per year) value, but are not exactly zero (the planets are not in mean motion resonance; in fact, there are no exact mean motion resonances between planets in the SS). If the associated coefficient (C_j) in the periodic term of the disturbing function is significant, then that term of the perturbation is important. For example, if only two planets have been taken into account, the periodic variations of Earth’s orbital elements depend on terms of the following form:

$$\sum_j \frac{C_j}{p n_i - q n_o} \sin((p n_i - q n_o) t + B_j) \quad (15)$$

where B_j is another coefficient depending on angular Keplerian elements. Hence, if an inequality is small and the amplitude C_j is important, we are in the presence of a significant perturbation, whose period is:

$$\text{Per}(p n_i - q n_o) = \frac{2\pi}{\text{ABS}(p n_i - q n_o)} = \text{ABS} \left(\frac{1}{\frac{p}{P_i} - \frac{q}{P_o}} \right) \quad (16)$$

where P_i and P_o are the orbital periods involved (note that $p = q = 1$ corresponds to the synodic periods of the pair of planets); ABS is the absolute value function. The smaller the significant inequality, the longer the associated perturbation period. In the SS the most important interaction is the Jupiter-Saturn (2:5) relationship, i.e., $2n_j - 5n_s \simeq -0.4 \frac{\text{deg.}}{\text{yr}}$, which leads to a

Great Inequality of period $\sim 800\text{-}1100$ yr (see e.g., Wilson, 1985); which was detected by Loutre et al. (1992) in the evolution of eccentricity.

In order to identify the planetary origin of these short periodicities, we need to evaluate the most important terms that produce detectable peaks in the spectral analysis of the Earth’s disturbing function, from Venus to, at least, Saturn. The simplest and most complete way in achieving this is to perform the high precision numerical simulations as provided by the MERCURY software package for orbital dynamics (Chambers, 1999) and then evaluate if any spectral peaks may be present (for a deep theoretical description and specific calculation of perturbations for a couple of planets the reader is directed to Simon, 1987). First, we integrate the Earth’s orbital motions adding only one planet at a time from Mercury to Saturn, to identify the “pure” periodicity of relevant perturbations; then we integrate the Earth with pairs of “related” planets (Venus + Mars; Jupiter + Saturn; etc.) to see the modification to these “pure” periodicities, and then all the relevant bodies (from Venus to Saturn) to see what, if any or all, of these short-term periodicities “are surviving” despite the predatory effects from stronger combined perturbations. By adopting this procedure we report in Fig. 9 that the prominent peaks related to planet Venus are (in the order of importance, i.e., spectral power):

$$3.98 \text{ yr} = \text{Per}(2V-3E); 2.67 \text{ yr} = \text{Per}(V-2E); 8.10 \text{ yr} = \text{Per}(3V-5E); 7.84 \text{ yr} = \text{Per}(5V-8E),$$

with V and E denote the mean motions of Venus and Earth. For the planet

Mars, the most conspicuous peak is:

$$15.76 \text{ yr} = \text{Per}(E-2\text{Ma}),$$

where Ma denotes the mean motion of Mars. In Fig. 9, the minor peaks labeled as P, P2 and P3, but with a confidence level less than 95%, come from Mars and correspond to the following periods:

$$2.47 \text{ yr} = \text{Per}(2E-3\text{Ma}); 2.9 \text{ yr} = \text{Per}(3E-5\text{Ma}); 5.25 \text{ yr} = \text{Per}(3(E-2\text{Ma})).$$

Peaks provided by Jupiter and Saturn mean motions ($\text{Per}(J) = 11.86 \text{ yr}$; $\text{Per}(S) = 29.4 \text{ yr}$) are also clearly visible. Of course the peaks around 6 yr and 14.7 yr are the second harmonics of J and S. The result of these short-term simulations are in good agreement with main result of previous works. It is important to note that the magnitude of the power spectrum cannot be taken as a direct indication of the perturbation intensity. Only an approximate estimation can be deduced from the raw data; the spectrum depends on detrending, sampling, etc., hence the relative intensity of two peaks can largely vary for the same phenomena, if the input data are processed straightforwardly.

Fig. 10 shows our MTM analysis (with a parabolic detrending of the raw, original data shown in Fig. 5) of the 13 kyr evolution of the record of eccentricity. All the peaks shown in Fig. 9 are detected in the detrended time series. Particularly, some peaks, such as the P, P2 and P3 are reinforced; raising above the 99% confidence level (note that P2 is immersed

in the power of the signal at around 2.7 yr). Some higher harmonics such as 4J, 3U (i.e., fourth and third harmonics of Jupiter and Uranus mean motions, respectively); P4 (the sixth harmonics of 8E-15Ma, ~ 41 yr); and P5 (fourth harmonics of the synodic period of Saturn and Neptune of ~ 36 yr), also appear. In particular, the perturbation with periodicities at around 3 yr strongly disturbs the (V-2E) periodicity and shifts this peak to 2.71 yr. Longitude of the perihelion or climatic precession shows basically the same periodicities (not shown). Notably, a spectral peak related to 4E-7Ma, not previously shown, is strongly present at around 3.56 yr. The other observed peaks are harmonics of the orbital frequencies present or non-linear combinations of the physical parameters' frequencies intervening in the definition of eccentricity.

Fig. 11 shows the MTM spectrum of obliquity from the detrended data record. Although a cubic-parabolic detrending have been applied to the raw series shown originally in Fig. 8, a secular trend in the spectral power is still present. This spectrum shows some common periodicities with the eccentricity and the precession of the perihelion signals. Periods directly coming from nutation are clearly detected, especially the period of lunar node (M_Ω), and the inequality 2E-3Ma, which comes from the direct part of planetary perturbation on Earth equatorial bulge (Souchay and Kinoshita, 1996, 1997; Souchay et al., 1999). Other direct planetary effects on nutation come from 4E-7Ma, and 3E-5Ma. In particular, a periodicity of 8.85 yr is clearly visible that is related to the second harmonic of Saturn-Uranus synodic frequency (period of about 17.9 yr), which produces considerable torque in the SS (see Cionco and Abuin, 2016). Nevertheless, this 8.85 yr

periodicity can also be related to the small perturbation of the Moon on the second order terrestrial potential J_3 (rigid Earth), with the argument $-l_M + F + M_\Omega$; where l_M is the mean anomaly of the Moon and $F = L_M - M_\Omega$, where L_M is the mean orbital longitude of the Moon.

In summary, all of the above-mentioned spectral peaks are by far the most important periodicities lesser than one century. Our solution DE431-IAU is more complete in covering all the periodicities that were previously known and shown; and some of these periods are expressed in daily insolation quantities which in turn should be studied for any relations to weather and climate as well as all the underlying physical processes.

7. Daily irradiance calculations

The daily irradiation or daily insolation, Q , for a whole rotational day of duration τ and the mean daily irradiance, W , at a given latitude, can be obtained by using Eq. (4), integrating over one full Earth's rotation, being the integral that is only significant when the Sun is over the horizon. In addition if we assume elements others than H to be unchanging over a whole day, the mean daily irradiance is:

$$\begin{aligned} W &= \frac{1}{2\pi} \int_{-\pi}^{\pi} I(\phi, \delta, r, H) dH \\ &= \text{TSI}_0 \left(\frac{1\text{au}}{r} \right)^2 \frac{2}{2\pi} \int_0^{H_s} (\sin \phi \sin \delta + \cos \phi \cos \delta \cos H) dH, \end{aligned} \quad (17)$$

where H_s is the sunset hour angle. Finally:

$$W = \frac{\text{TSI}_0}{\pi} \left(\frac{1\text{au}}{r} \right)^2 (H_s \sin \phi \sin \delta + \cos \phi \cos \delta \sin H_s), \quad (18)$$

reckoned in the same units as TSI_0 (W m^{-2}). In addition, Eq. (4) permits one to find the daily amount of solar irradiance between the time of sunrise (t_s) and sunset (t_p) which is:

$$Q = \text{TSI}_0 \left(\frac{1\text{au}}{r} \right)^2 \int_{t_s}^{t_p} (\sin \phi \sin \delta + \cos \phi \cos \delta \cos H) dt, \quad (19)$$

if we assume t to be the mean solar-time timescale (i.e., we drop the difference with true solar time); using the rotational relationship with H (1 mean day of τ seconds):

$$H = \frac{2\pi}{\tau}(t - t_o), \quad (20)$$

then:

$$Q = \frac{\tau}{\pi} \text{TSI}_0 \left(\frac{1\text{au}}{r} \right)^2 \int_0^{H_s} (\sin \phi \sin \delta + \cos \phi \cos \delta \cos H) dH, \quad (21)$$

for one solar day of $\tau = 86400$ s; and assuming the constancy of the Sun declination, Q becomes:

$$Q = \frac{86400}{\pi} \text{TSI}_0 \left(\frac{1\text{au}}{r} \right)^2 (H_s \sin \phi \sin \delta + \cos \phi \cos \delta \sin H_s), \quad (22)$$

which is expressed in J m^{-2} , if TSI_0 is in W m^{-2} . Eq. (3) permits one to find the value of the H at sunrise-sunset. When the Sun is on the horizon (i.e., Sun at 90 deg. of the zenith) the dot product is zero, hence:

$$\cos(H_s) = -\tan \phi \tan \delta. \quad (23)$$

Eq. (23) acts as a discriminant for sunrise-sunset. If we call $D = -\tan \phi \tan \delta$, then the Sun rises and sets at certain latitude when:

$$-1 \leq D \leq 1. \quad (24)$$

If $D = -1$ for a particular observer; the Sun is at the limit of rising and setting; i.e., when $H_s = \pm 180$ deg.; the Sun becomes circumpolar for that observer: no sunrise-sunset for the time-span during $D < -1$. Of course, this occurs when ϕ and δ have the same sign (the Sun at the same hemispheric position). Then if:

$$D < -1, \quad (25)$$

the Sun does not set (polar day). When the Sun's declination changes sign, the winter season arrives, and H_s decreases, and for certain latitude, it is virtually zero; then $D = 1$. Therefore, the Sun does not rise (polar night), if:

$$D > 1, \quad (26)$$

and insolation quantities are null. If $D < -1$, then the integrand in Eq. (17) is significant over 0 to 2π ; hence, the mean irradiance for the circumpolar Sun is:

$$\begin{aligned} W_c &= \text{TSI}_0 \left(\frac{1\text{au}}{r} \right)^2 \frac{1}{2\pi} \int_0^{2\pi} (\sin \phi \sin \delta + \cos \phi \cos \delta \cos H) dH \\ &= \text{TSI}_0 \left(\frac{1\text{au}}{r} \right)^2 \sin \phi \sin \delta. \end{aligned} \quad (27)$$

Then, Eq. (19) becomes:

$$\begin{aligned}
Q_c &= \text{TSI}_0 \left(\frac{1\text{au}}{r} \right)^2 \frac{86400}{2\pi} \int_0^{2\pi} (\sin \phi \sin \delta + \cos \phi \cos \delta \cos H) dH \\
&= 86400 \text{TSI}_0 \left(\frac{1\text{au}}{r} \right)^2 \sin \phi \sin \delta.
\end{aligned} \tag{28}$$

Therefore, using Eq. (23) as discriminant, we can calculate by means of Eqs. (18, 22, 27, 28), these daily solar quantities, knowing all of the other corresponding solar-terrestrial parameters for a certain date. As a matter of consistency, we see that the averaged quantities can be directly obtained in dividing the daily values by 86400 ($W = Q/86400$).

In the derivation of Eqs. (18, 22, 27, 28) we adopted a day-based approach, i.e., taking the longitude data tabulated (at noon) for that date. This particular approach is the conventional procedure commonly used in obtaining daily solar quantities (see e.g., Berger, 1988; Laskar et al., 1993; Berger et al., 2010). Nevertheless, as we have hinted at the beginning of this article, it is an usual practise in paleoclimate studies, to calculate Q (or W) by fixing the Earth/Sun position at an arbitrary moment; i.e., fixing an arbitrary value of solar longitude inside a particular day; this is equivalent to taking Eqs. (18, 22, 27, 28) as a continuous function of longitudes. For example, to follow the daily irradiation at March equinox for a mid-latitude observer, the Eq. (18) is used by setting $\lambda_{\odot t} = 0$ as a temporal reference in Eq. (5), to find δ . This approach is understandable because at ancient time we do not know these parameters “exactly” at noon. Moreover, we can assume that the change of solar longitude inside a day does not significantly affect the estimate of daily insolation (Berger et al., 2010). Nevertheless, we consider the clarification and recognition of this assumption to be important

for all users of available databases of solar irradiation (see next Sub-Section 77.1).

Fig. 12 shows the daily mean irradiation at equinoxes ($\lambda_{\odot t} = 0, 180$ deg.), using our DE431-IAU solution, over the indicated calendar time, at 65°N . The solar constant used is 1366 W m^{-2} . Fig. 13 shows similar quantities as in Fig. 12 but for solstices; i.e., $\lambda_{\odot t} = 90, 270$ deg. Both calculations were performed taking Eq. (18) as a continuous function of solar longitude. As were pointed out by Borisenkov et al. (1983) and Loutre et al. (1992), the secular long-term modulation by precession is evident for equinoxes, even at high latitudes. For solstices the dominant signal is provided by the modulation of the obliquity variations. For daily insolation calculations, we prepare a FORTRAN code that calculates Q and W (Eqs. 18, 22, 27, 28) along the time for a specific solar longitude and latitude on Earth. The code `INSOLA-Q-W.for` permits the calculation of Q or W for the exact mid-day at the tabulated longitude of a certain Julian day, or to set Q or W as continuous functions of the solar longitude, which is the common practice in paleoclimate studies. Fig. 12 and 13 were made with this last strategy, i.e., by setting $\lambda_{\odot t}$ with the desired value (0, 90, 180 or 270 deg.) using Eq. (18) and (22), but taking the DE431-IAU elements for the specific tabulated JD within which the corresponding value, in our cases of equinoxes or solstices, occurs. Hence, these values were calculated for the specific astro-climatic parameters of the corresponding mid-day, but did not used the tabulated mid-day longitude, as daily insolation should be calculated in theory. The difference between the desired longitude and the tabulated mid-day value can reach $\sim \pm 0.7$ deg.

Fig. 14 shows W at the “mid-month” of July; i.e., $\lambda_{\odot t} = 120$ deg. In

keeping with the usual practice in paleoclimate, we are continuing to adopt the present calendar defining mid-month moments at an angular step of 30 deg., from March (0 deg.) to February (330 deg.). Then the calculation was also performed taking W as a continuous function of $\lambda_{\odot t}$. The period corresponds to the same interval considered in Figure 12a of Loutre et al. (1992), from 1450 AD to 1950 AD. In fact, this permits a direct comparison of our result with Loutre et al. (1992); and this comparison yields a very good agreement. We do not know the precise TSI_0 value adopted by those authors (but we presumed it was about $1366\text{-}1367 \text{ W m}^{-2}$ during solar activity minima as hinted on p. 191 of Loutre et al. 1992), but this level of agreement is reached with 1366 W m^{-2} . The obliquity signal is prominently present, with the two main periodicities clearly visible: the ~ 20 yr oscillation due to lunar retro-gradating motion (18.6 yr) and the strong $\sim 2\text{-}3$ yr period.

With regards to other periodicities, we performed an extensive spectral analysis on daily insolation outputs (using detrended time series), especially focused at the shortest periodicities on biennial to 40 yr timescales (the main periods present in astro-climatic elements). For a comparison with Loutre et al. (1992), we show the results for July mid-month at 65°N (Fig. 15). Several periods visible in the eccentricity, longitude of the perihelion and obliquity signals are present, but also prominent harmonics and non-linear interactions of frequencies present in the parameters that define daily insolation. The shortest periods oscillate at about 2.42 yr and 2.69 yr and correspond to the perturbed periods by 2E-3Ma and V-2E, respectively. At around 3 yr there are several harmonics and 3E-5Ma (2.9 yr), 4E-7Ma (3.56 yr), 4J; etc. Then 3.98 yr (2V-3E); 5.26 yr (3(E-2Ma)); 2J; 7.88 yr (5V-8E);

8.09 yr (3V-5E); Per(J); Per($2 M_\Omega$), Per(2S), Per(M_Ω) and Per(S) complete the most important periods present. For lower latitudes (e.g., 0 deg.), the spectrum is essentially the same; the only change is the attenuation of the obliquity signal; as expected because precession signal is dominant at tropical latitudes. At these lower latitudes, the 18.6 yr period and its harmonics appears smaller than, for example, the Jupiter signal.

Although our derived periodicities are similar to Loutre et al. (1992), we found a richer set of periodicities at around 2-3 yr, 5 yr, and 8 yr, coming from a more complete description of planetary perturbations performed in DE431 and also the more complete model of nutation. Also, by performing a much more detailed detrending and sampling, we can also produce similar results as those discussed in Loutre et al. (1992) for the longest periodicities covering oscillations on timescales from multiculturies to a millennium.

In addition, we have created another code `MONTH-GEO.for` designed to calculate the geographical distribution of mid-month insolation for arbitrary years (between -10 kyr, 3 kyr), in different latitudinal bands. An output for the year 1650, near the beginning of the Maunder Minimum, can be seen in Table 1, for the indicated latitudes. This code calculates W , as continuous functions of $\lambda_{\odot t}$, i.e., at the corresponding longitudes for each mid-month of the conventional calendar. All our codes are available with the publication of this paper.

7.1. The effect of the non-constant longitude within a day

As discussed in details in the previous section, Q and W formulas were derived assuming that we have astro-climatic elements and true orbital longitudes at solar noon ($H = 0$) and these values do not change significantly

over a complete 2π variation of H . This approximation is supposed to lead to a maximum theoretical error of 0.01 W m^{-2} in the determinations of W (Berger et al., 2010).

In our STOF calculations, we know the value of the true solar longitude at mid-day and the astro-climatic elements for that day. Therefore, we can estimate the difference or “error” in the estimation of corresponding solar quantity between the exact tabulated value at mid-day (Q_0 and W_0) and the estimation considering Q or W as a continuous function of $\lambda_{\odot t}$: the difference, $Q - Q_0$, $W - W_0$ and also the “relative error” ratio, $(Q - Q_0)/Q_0 = (W - W_0)/W_0$. As far as we know, these differences have not been discussed nor addressed in the literature.

To describe these differences as a function of time, we have shown in Fig. 16 and 17 (for 65°N) the relative error ratios evaluated at equinoxes and solstices for all the 13 kyr studied period. At the solstices, when the Sun is stationary, the relative errors are small. Although there are values as large as 0.2%, they are all mostly less than 0.1%. For the equinoxes the relative differences are larger, reaching $\pm 1.2\%$. Evidently, we are confirming that the characteristic of this relative error is dependent on solar longitude. To explore this, we calculate this error as a function of longitude for every 10-degree interval. The result is shown in Fig. 18. We observe very large relative differences of up to $\pm 5\%$ around December solstice.

The biggest relative differences between nominal Q or W values and the corresponding values as continuous functions of time, occur at the moment when the Sun is near the extreme declination at opposite hemispheres. This means that these big relative errors occur in the seasons when the insolation

values are near minimum (of course, the same occurs for a southern observer); then, there are not so important differences on the amount of modeled received energy at these moments, as we can see in Fig. 19, where W values (in continuous and tabulated modes) for $\lambda_{\odot t} = 250$ deg. (i.e., November-December), are depicted for the last 1 kyr. Nevertheless, as we can see in Fig. 20, this error for the mean daily insolation, can increase up to $\sim 2.5 \text{ W m}^{-2}$ in absolute values. These largest errors occur after the March equinox (at the beginning of the boreal spring) and at the end of the boreal summer. The behavior of these differences depends strictly on the trigonometric part of Eq. (18), which is a monotonically increasing function of declination, which varies approximately between 7×10^{-3} and 1 between December and June, respectively, for a northern observer. The smallest errors are occurring around solstice of December because of the very small differences resulting from the subtraction between two smallest values of this function. Conversely, slightly larger errors with respect to December solstice, occur near solstice of June, when the expression for the trigonometric function in Eq. (18) has its largest values.

The characteristics of this error is similar as a function time, over the full 13 kyr interval studied. Of course, this error could lead to large differences for initial conditions in a climatic modeling code especially when the climatic system is evolving nonlinearly while encountering the chaotic regime of the climate dynamic phase space. Therefore, the difference in evaluating Q or W as continuous functions of longitudes or tabulated values, provides a clue of the “uncertainty” associated with the correct incoming solar radiation when the daily insolation value is basically a *guess* in connection to climate

modeling.

7.2. Comparison with the state of the art works by J. Laskar and colleagues

The longest database available for Milanković orbital forcing is the one provided by Laskar et al. (2004), and its extension to -250 Myr in Laskar et al. (2011a). While this solution in astro-climatic elements is given for -250 Myr from present, inherent problems to its chaotic evolution make it strictly valid, in paleoclimate studies, over about -50 Myr and $+20$ Myr from the present, which is the time-span covered by former Laskar et al. (2004) solution. This French solution (available at NOAA/NCDC which redirect to L'Institut de Mécanique Céleste et de Calcul des Éphémérides -IMCCE-) is consistent with Berger and Loutre (1991) for the last 5 Myr where latter was, in turn, based on the original Laskar (1986, 1988) results. This is the reason we have considered only the solution calculated by Laskar and colleagues which we have labeled here as La2010 solution, as the authors named their last solution in the paper of the year 2011 for a comparison to our DE341-IAU solution. The comparison also allows indirect assessments of Berger and Loutre solutions. The web interface at IMCEE, permits outputs from -100 Myr to $+20$ Myr from J2000.0, but at a minimum timestep of 100 yr; hence this is the maximal resolution of this data that we took into account, which is fine enough for our purposes.

We compare mean daily insolation at July mid-month (i.e., $\lambda_{\odot t} = 120$ deg.) for 65°N , i.e., as a continuous function of longitude, using the `INSOLA-Q-W.for` code. Fig. 21 shows this calculation for 12 kyr, from year -10000.0 to 2000.0 . Whereas our results describe the short-term variations on W , La2010 solution describes the mean variations (to make our results clearly visible at this

scale, we have decided do not graph La2010 solution from -12 kyr to -10 kyr, which describes the mean values of our DE431-IAU solution). A zoom between -10 kyr and -9.6 kyr from J2000.0, shows the excellent agreement of our result with La2010, and the effects of STOF on W . To show the differences between continuous and tabulated values in our DE431-IAU solution, we performed the same calculation, using tabulated values at mid-day. Fig. 22 shows these differences in detail for the past 1 kyr. There are differences up to $\pm 0.3\%$ which represents a maximum error of about 1.2 W m^{-2} for this particular July mid-month calculation. Hence, a user that calculated the mean daily insolation using La2010 solution, can have an error up to 1.2 W m^{-2} considering solar position at the noon time of the corresponding day, for July mid-month.

As a final commentary, Loutre et al. (1992) had shown that the level of disagreement of their solution with the original solution from Berger (1978) can be as large as 10 W m^{-2} for 10 kyr to 5 kyr before 1950 AD; while the disagreement is more tolerable at level of less than 1 W m^{-2} for 5 kyr to present. Hence, our work presents a better agreement with respect to the state of the art solution by Laskar et al. (2011a). Our STOF solutions do not show evidence for any long-term growth in comparison to the La2010 solution; La2010 describes virtually the mean value of our STOF solution. The departure of our (continuously-varying-longitude) solution with respects to secular variations are indeed small, less than about $\pm 0.15 \text{ W m}^{-2}$ over the full Holocene interval covered in our DE431-IAU solution. As an example, for this July comparison, the long-term La2010 value corresponding to -1 kyr from J2000.0 (obtained from web interface) is $W = 430.162 \text{ W m}^{-2}$, keeping

three decimal figures; our DE431-IAU solution (in continuous mode), for mid-July, i.e., with $\lambda_{\odot t} = 120$ deg. (which correspond to $t = 1000.577$ yr of our solution, with a true mid-day longitude of $\lambda_{\odot t} = 119.673$ deg.) give us $W = 430.238 \text{ W m}^{-2}$, a difference of less than -0.018% . For -10 kyr from J2000.0, La2010 gives $W = 468.978 \text{ W m}^{-2}$, whereas our solution gives $W = 468.968 \text{ W m}^{-2}$ (at $t = -8000.2382$ yr), a difference of $\sim 0.002\%$. This independent confirmation suggests that our solution can be applied for exploring any climate modeling experiments accounting fully for the STOF aspects of the orbital forcings previously not available publicly.

8. Summary

We have presented a new set of calculations accurately accounting for all short-term orbital modulations that can be considered an improved representation of the boundary conditions relevant for any meteorological and climatic studies over the Holocene interval and 1 kyr into the future. We have reviewed the subject carefully and discussed all the steps and assumptions involved in our calculations. Our new orbital solutions, DE341-IAU, offer an internally self-consistent set of boundary conditions readily applicable for climate model simulation, attribution and even assimilation studies. The rich spatio-temporal dynamics of the persistent solar irradiation forcing offers a realistic accounting of all STOF dynamics suitable for the evaluation of all atmospheric, oceanic and coupled air-sea oscillations on timescales ranging from diurnal, fortnightly, monthly, sub-annual, seasonal, annual, QBO, ENSO, decadal to multidecadal timescales.

We offer, for the first time, a detailed determination of the error com-

mitted using daily insolation quantities as a continuously varying longitude over the day (i.e., the most common practice in all paleoclimate modeling study thus far) with respect to the nominal (based on solar position at noon) values. We found errors up to 5% in daily insolation quantities, which correspond to an absolute difference of 2.5 W m^{-2} in W calculations, which are significantly larger than the theoretically expected error (i.e., 0.01 W m^{-2} reported in Berger et al., 2010) in the calculation of W . This error is of similar order as the uncertainty detected by Jousaume and Braconnot (1997) due to the “calendar effects” (i.e., $5\text{-}8 \text{ W m}^{-2}$), which have been shown to be considerably consequential on climate modeling (see also Chen et al., 2011). However, when compared to the relatively well-documented calendar effect, it is important to note that our continuous-versus-tabulated longitude error is a different effect which can occur even in the same specific calendar day. Therefore, climate modelers have to be aware of these differences and how this particular error would spread and propagate along with time especially when intra-annual insolation quantities are required. The sensitivity of initial climate conditions to these differences should also be addressed.

Our next step will be to incorporate a range of estimates of intrinsic changes in TSI for the past few thousand years as constrained both by solar activity proxies from paleoclimatic evidence as well as observational study of solar-type stars. The astro-climatic parameters database, the FORTRAN codes and all the solar radiation values will be made available to any scientists and climate modeling groups requesting for them. We will also make effort to install our solar radiation forcing outputs on several popular data archive centers including the one at NOAA/NCDC. Finally, after the com-

pletion of our calculation, we discover that another parallel and independent effort on tackling STOF has been ongoing in Russia by Fedorov (2015) where the author adopted the JPL DE 405/406 Planetary and Lunar Ephemerides covering the time interval from 3000 BC to 2999 AD.

Acknowledgments

The authors acknowledge the support of the grant UTN-3577 “Efectos Orbitales sobre la Irradiancia Solar Recibida Durante el Holoceno y los Próximos 3000 Años” (2015-2016) of the Universidad Tecnológica Nacional, Argentina. The authors are indebted to William Folkner of NASA-JPL, for an open and deep discussion of DE-JPL ephemerides models and details. We also extend thanks to Jean-Louis Simon of Paris Observatory-IMCEE, France, for sharing one of his papers and valuable commentaries. Special thanks to John Chambers of Carnegie Institution of Washington, for sharing his Julian Day routine that is especially useful for negative years. Finally, we are grateful to Maria McEachern, the librarian at the John Wolbach library of the Center for Astrophysics, for valuable help. W.S.’s work is indirectly supported by SAO grant proposal ID 000000000003010-V101. W.S. would also like to acknowledge the influence by Dr. Duncan Steel’s independent examination of the STOF question and to thank the late Bob Carter, Milan Dimitrijevic, Monika Jurkovic, Laszlo Kiss, Katalin Olah, and Dmitry Sokoloff for helps and encouragements.

References

- Berger, A., 1978. Long-term variations of daily insolation and Quaternary climatic changes. *Journal of the Atmospheric Sciences* 35 (12), 2362–2367.
- Berger, A., 1988. Milankovitch theory and climate. *Reviews of Geophysics* 26, 624–657.
- Berger, A., 2012. A brief history of the astronomical theories of paleoclimates. In: *Climate Change*. Springer, pp. 107–129.
- Berger, A., Loutre, M. F., 1991. Insolation values for the climate of the last 10 million years. *Quaternary Science Reviews* 10, 297–317.
- Berger, A., Loutre, M.-F., Yin, Q., 2010. Total irradiation during any time interval of the year using elliptic integrals. *Quaternary Science Reviews* 29 (17), 1968–1982.
- Bertrand, C., Loutre, M.-F., Berger, A., 2002. High frequency variations of the Earth's orbital parameters and climate change. *Geophysical Research Letters* 29 (18), 40–1–40–4.
- Borisenkov, Y. P., Tsvetkov, A., Agaponov, S., 1983. On some characteristics of insolation changes in the past and the future. *Climatic Change* 5 (3), 237–244.
- Borisenkov, Y. P., Tsvetkov, A., Eddy, J. A., 1985. Combined effects of earth orbit perturbations and solar activity on terrestrial insolation. Part I: Sample days and annual mean values. *Journal of the Atmospheric Sciences* 42 (9), 933–940.

- Bretagnon, P., Jan. 1974. Termes a longues périodes dans le système solaire. *Astronomy & Astrophysics* 30, 141–154.
- Bretagnon, P., Oct. 1982. Theory for the motion of all the planets - The VSOP82 solution. *Astronomy & Astrophysics* 114, 278–288.
- Capitaine, N., Soffel, M., Aug. 2015. On the definition and use of the ecliptic in modern astronomy. In: Malkin, Z., Capitaine, N. (Eds.), *Journées 2014 "Systèmes de référence spatio-temporels"*. pp. 61–64.
- Chambers, J. E., 1999. A hybrid symplectic integrator that permits close encounters between massive bodies. *Monthly Notices of the Royal Astronomical Society* 304 (4), 793–799.
- Chen, G.-S., Kutzbach, J., Gallimore, R., Liu, Z., 2011. Calendar effect on phase study in paleoclimate transient simulation with orbital forcing. *Climate dynamics* 37 (9-10), 1949–1960.
- Cionco, R. G., Abuin, P., 2016. On planetary torque signals and sub-decadal frequencies in the discharges of large rivers. *Advances in Space Research* 57 (6), 1411–1425.
- Collins, M., Knutti, R., Arblaster, J., Dufresne, J.-L., Fichet, T., Friedlingstein, P., Gao, X., Gutowski, W., Johns, T., Krinner, G., Shongwe, M., Tebaldi, C., Weaver, A., Wehner, M., 2013. Long-term climate change: Projections, commitments and irreversibility. In: Stocker, T., Qin, D., Plattner, G.-K., Tignor, M., Allen, S., Boschung, J., Nauels, A., Xia, Y., Bex, V., Midgley, P. (Eds.), *Climate Change 2013: The Physical Science Basis. Contribution of Working Group I to the Fifth Assessment Report*

- of the Intergovernmental Panel on Climate Change. Cambridge University Press, Cambridge, United Kingdom and New York, NY, USA, p. 10291136. URL www.climatechange2013.org
- Cronin, T. W., 2014. On the choice of average solar zenith angle. *Journal of the Atmospheric Sciences* 71 (8), 2994–3003.
- Duriez, L., 2002. *Cours de Mécanique Céleste classique*. Laboratoire d'astronomie de l'université de Lille 1.
- Essex, C., 2011. Climate theory versus a theory for climate. *International Journal of Bifurcation and Chaos* 21, 3477–3487.
- Fedorov, V., 2015. Spatial and temporal variations in solar climate of the Earth in the present epoch. *Izvestiya, Atmospheric and Oceanic Physics* 51 (8), 779–791.
- Fienga, A., Manche, H., Laskar, J., Gastineau, M., Jan. 2008. INPOP06: a new numerical planetary ephemeris. *Astronomy & Astrophysics* 477, 315–327.
- Folkner, W. M., Williams, J. G., Boggs, D. H., Park, R. S., Kuchynka, P., Feb. 2014. The planetary and lunar ephemerides DE430 and DE431. *Interplanetary Network Progress Report* 196, 1–81.
- Ghil, M., Allen, M. R., Dettinger, M. D., Ide, K., Kondrashov, D., Mann, M. E., Robertson, A. W., Saunders, A., Tian, Y., Varadi, F., Yiou, P., Feb. 2002. Advanced spectral methods for climatic time series. *Reviews of Geophysics* 40, 3–1–3–41.

- Goody, R., 2007. Maximum entropy production in climate theory. *Journal of the Atmospheric Sciences* 64 (7), 2735–2739.
- Hansen, J. M., Aagaard, T., Kuijpers, A., 2015. Sea-level forcing by synchronization of 56-and 74-year oscillations with the Moon’s nodal tide on the northwest European shelf (eastern North Sea to central Baltic Sea). *Journal of Coastal Research* 31 (5), 1041–1056.
- He, B., Wu, G., Liu, Y., Bao, Q., 2015. Astronomical and hydrological perspective of mountain impacts on the Asian summer monsoon. *Scientific Reports* 5.
- Hersbach, H., Peubey, C., Simmons, A., Berrisford, P., Poli, P., Dee, D., 2015. Era-20cm: a twentieth-century atmospheric model ensemble. *Quarterly Journal of the Royal Meteorological Society* 141 (691), 2350–2375.
- Hogan, R. J., Hirahara, S., 2016. Effect of solar zenith angle specification in models on mean shortwave fluxes and stratospheric temperatures. *Geophysical Research Letters* 43 (1), 482–488.
- Hudson, T., Horseman, A., Sugier, J., 2016. Diurnal, seasonal and 11-yr solar cycle variation effects on the virtual ionosphere reflection height and implications for the met office’s lightning detection system, ATDnet. *Journal of Atmospheric and Oceanic Technology* 33, 1429–1441.
- IAU SOFA Board, 2016. IAU SOFA software collection.
URL <http://www.iausofa.org>
- Imbrie, J., 1982. Astronomical theory of the Pleistocene ice ages: A brief historical review. *Icarus* 50 (2), 408–422.

- Jajcay, N., Hlinka, J., Kravtsov, S., Tsonis, A. A., Paluš, M., 2016. Time scales of the European surface air temperature variability: The role of the 7–8 year cycle. *Geophysical Research Letters* 43 (2), 902–909.
- Ji, F., Wu, Z., Huang, J., Chassignet, E. P., 2014. Evolution of land surface air temperature trend. *Nature Climate Change* 4, 462–466.
- Joussaume, S., Braconnot, P., 1997. Sensitivity of paleoclimate simulation results to season definitions. *Journal of Geophysical Research: Atmospheres* 102 (D2), 1943–1956.
- Kaplan, G. H., 2006. The IAU resolutions on astronomical reference systems, time scales, and Earth rotation models. arXiv preprint astro-ph/0602086.
- Kinoshita, H., 1977. Theory of the rotation of the rigid Earth. *Celestial Mechanics* 15 (3), 277–326.
- Laskar, J., Mar. 1986. Secular terms of classical planetary theories using the results of general theory. *Astronomy & Astrophysics* 157, 59–70.
- Laskar, J., Jun. 1988. Secular evolution of the solar system over 10 million years. *Astronomy & Astrophysics* 198, 341–362.
- Laskar, J., 2013. Is the solar system stable? In: Duplantier, B., Nonnenmacher, S., Rivasseau, V. (Eds.), *Chaos*. Springer, pp. 239–270.
- Laskar, J., Fienga, A., Gastineau, M., Manche, H., 2011a. La2010: a new orbital solution for the long-term motion of the Earth. *Astronomy & Astrophysics* 532, A89.

- Laskar, J., Gastineau, M., Delisle, J.-B., Farres, A., Fienga, A., 2011b. Strong chaos induced by close encounters with Ceres and Vesta. *Astronomy & Astrophysics* 532, L4.
- Laskar, J., Joutel, F., Boudin, F., 1993. Orbital, precessional, and insolation quantities for the Earth from -20 Myr to +10 Myr. *Astronomy & Astrophysics* 270, 522–533.
- Laskar, J., Robutel, P., Joutel, F., Gastineau, M., Correia, A., Levrard, B., 2004. A long-term numerical solution for the insolation quantities of the Earth. *Astronomy & Astrophysics* 428 (1), 261–285.
- Li, Y., Han, W., Shinoda, T., Wang, C., Lien, R.-C., Moum, J. N., Wang, J.-W., 2013. Effects of the diurnal cycle in solar radiation on the tropical indian ocean mixed layer variability during wintertime madden-julian oscillations. *Journal of Geophysical Research: Oceans* 118 (10), 4945–4964.
- Lieske, J., Lederle, T., Fricke, W., Morando, B., 1977. Expressions for the precession quantities based upon the IAU/1976/system of astronomical constants. *Astronomy & Astrophysics* 58, 1–16.
- Lin, M., Huybers, P., 2016. Revisiting whether recent surface temperature trends agreed with the CMIP5 ensemble. *Journal of Climate*, in press.
- Lions, J., Manley, O., Temam, R., Wang, S., 1997. Physical interpretation of the attractor dimension for the primitive equations of atmospheric circulation. *Journal of the Atmospheric Sciences* 54 (9), 1137–1143.

- Loutre, M.-F., Berger, A., Bretagnon, P., Blanc, P.-L., 1992. Astronomical frequencies for climate research at the decadal to century time scale. *Climate Dynamics* 7 (4), 181–194.
- Mathews, P. M., Herring, T. A., Buffett, B. A., 2002. Modeling of nutation and precession: new nutation series for nonrigid Earth and insights into the Earth’s interior. *Journal of Geophysical Research: Solid Earth* 107 (B4).
- Mekaoui, S., Dewitte, S., Conscience, C., Chevalier, A., 2010. Total solar irradiance absolute level from DIARAD/SOVIM on the International Space Station. *Advances in Space Research* 45 (11), 1393–1406.
- Milanković, M., 1941. *Kanon der erdbestrahlung und seine anwendung auf das eiszeitenproblem* (Canon of Insolation and the Ice-Age Problem). Acad. Roy. Serbian, Editions spec (1969 translation by the Israel Program for Scientific Translation; Edited by B. Benny and I. Meroz) 133, 1–484.
- Miller, R. L., Schmidt, G. A., Nazarenko, L. S., co authors, Apr. 2014. CMIP5 historical simulations (1850-2012) with GISS ModelE2. *Journal of Advances in Modeling Earth Systems* 6, 441–477.
- Monin, A. S., Shishkov, Y. A., Apr. 2000. Reviews of topical problems: Climate as a problem of physics. *Physics Uspekhi* 43, 381–406.
- Morrison, L. V., Stephenson, F. R., 2004. Historical values of the Earth’s clock error Δt and the calculation of eclipses. *Journal for the History of Astronomy* 35, 327–336.
- Murray, C. D., Dermott, S. F., 1999. *Solar system dynamics*. Cambridge Univ. Press.

- Neumann, J., 1985. Climatic change as a topic in the classical greek and roman literature. *Climatic Change* 7 (4), 441–454.
- Nicolis, C., Nicolis, G., 1995. From short-scale atmospheric variability to global climate dynamics: toward a systematic theory of averaging. *Journal of the Atmospheric Sciences* 52 (11), 1903–1913.
- Owen, W. M., 1990. A theory of the Earth’s precession relative to the invariable plane of the Solar System. Ph.D. thesis, University of Florida.
- Petrović, A., 2009. Revolution and insolation: How Milutin Milanković has assembled the puzzle of the climate? *Scientific Technical Review* 59 (1), 3–10.
- Pitjeva, E. V., Pitjev, N. P., Aug. 2014. Development of planetary ephemerides EPM and their applications. *Celestial Mechanics and Dynamical Astronomy* 119, 237–256.
- Roy, A. E., 1978. *Orbital motion*. IOP Publishing Ltd.
- Sharaf, S. G., Boudnikova, N., 1967. Secular variations of elements of the Earth’s orbit which influences the climates of the geological past. *Bull. Inst. Teor. Astron. Akad. Nauk SSSR* 11, 231–261.
- Shinoda, T., 2005. Impact of diurnal cycle of solar radiation on intraseasonal SST variability in the Western Equatorial Pacific. *Journal of Climate* 18, 2628–2636.
- Simmons, A., Poli, P., Dee, D., Berrisford, P., Hersbach, H., Kobayashi, S., Peubey, C., 2014. Estimating low-frequency variability and trends in atmo-

- spheric temperature using ERA-Interim. *Quarterly Journal of the Royal Meteorological Society* 140 (679), 329–353.
- Simon, J.-L., Mar. 1987. Computation of the first and second derivatives of the Lagrange equations by harmonic analysis. *Astronomy & Astrophysics* 175, 303–308.
- Simon, J.-L., Francou, G., Fienga, A., Manche, H., 2013. New analytical planetary theories VSOP2013 and TOP2013. *Astronomy & Astrophysics* 557, A49.
- Soon, W., 2014. Sun shunned. In: Moran, A. (Ed.), *Climate Change: The Facts 2014*. Institute of Public Affairs, pp. 57–66.
- Soon, W., Connolly, R., Connolly, M., 2015. Re-evaluating the role of solar variability on northern hemisphere temperature trends since the 19th century. *Earth-Science Reviews* 150, 409–452.
- Souchay, J., Kinoshita, H., Aug. 1996. Corrections and new developments in rigid Earth nutation theory. I. Lunisolar influence including indirect planetary effects. *Astronomy & Astrophysics* 312, 1017–1030.
- Souchay, J., Kinoshita, H., Feb. 1997. Corrections and new developments in rigid-Earth nutation theory. II. Influence of second-order geopotential and direct planetary effect. *Astronomy & Astrophysics* 318, 639–652.
- Souchay, J., Loysel, B., Kinoshita, H., Folgueira, M., Feb. 1999. Corrections and new developments in rigid Earth nutation theory. III. Final tables “REN-2000” including crossed-nutation and spin-orbit coupling effects. *Astronomy & Astrophysics Supplement* 135, 111–131.

- Standish, Jr., E. M., Oct. 1982. Orientation of the JPL Ephemerides, DE 200/LE 200, to the dynamical equinox of J2000. *Astronomy & Astrophysics* 114, 297–302.
- Steel, D., 2013. Perihelion precession, polar ice and global warming. *Journal of Cosmology* 22, 10106–10129.
- Trenberth, K. E., Fasullo, J. T., von Schuckmann, K., Cheng, L., 2016. Insights into Earth’s energy imbalance from multiple sources. *Journal of Climate*, in press.
- Vondrák, J., Capitaine, N., Wallace, P., 2011. New precession expressions, valid for long time intervals. *Astronomy & Astrophysics* 534, A22.
- Wilson, C., 1985. The great inequality of Jupiter and Saturn: from Kepler to Laplace. *Archive for History of Exact Sciences* 33, 15–290.

Table LIST - CAPTIONS

Table 1: Mid-month W values at indicated latitudinal bands, for the year 1650, at the beginning of the Maunder Minimum interval of reduced sunspot activity; $TSI_0 = 1366.0 \text{ W m}^{-2}$ (code MONTH – GEO.for). Each file corresponds to one month, from March to February.

Table 1: Mid-month W values at indicated latitudinal bands, for the year 1650, at the beginning of the Maunder Minimum interval of reduced sunspot activity; $TSI_0 = 1366.0 \text{ W m}^{-2}$ (code MONTH – GEO.for). Each file corresponds to one month, from March to February.

80°S	65°S	35°S	0°	35°N	65°N	80°N
479.093	457.392	495.965	421.104	216.929	16.487	0.000
273.664	327.543	439.656	435.016	280.267	75.693	0.000
75.854	184.610	357.826	436.825	357.826	184.610	75.854
0.000	73.207	271.054	420.713	425.199	316.770	264.660
0.000	15.558	204.709	397.381	468.027	431.626	452.106
0.000	2.744	179.712	385.755	481.757	480.005	518.599
0.000	15.497	203.867	395.742	466.091	429.836	450.227
0.000	72.683	269.130	417.732	422.190	314.535	262.799
75.240	183.117	354.932	433.292	354.932	183.117	75.240
271.797	325.287	436.611	431.991	278.309	75.155	0.000
477.195	455.571	493.975	419.403	216.045	16.413	0.000
554.521	513.252	515.122	412.469	192.155	2.933	0.000

FIGURES LIST - CAPTIONS (ALL FIGURES IN BLACK-WHITE)

Fig. 1: A local fixed geocentric equatorial system (X, Y, Z) is defined; X directed towards the local meridian; minus Z axis directed towards the hemispheric pole (south, here). The minus Y axis points west. The positions of the observer's zenith and the Sun are also indicated.

Fig. 2: Sketch of the Earth's orbit in the present time (reference epoch J2000.0). The Sun (with the usual astronomical symbol \odot) is at the focus. Nevertheless, to describe the apparent (also anti-clockwise), relative movements of the Sun with respect to Earth, we have marked the Sun projections on the celestial sphere, specially for the corresponding solstices and equinoxes, which permit a determination of λ_{\odot} to be used in the insolation formulas. Also, the effect of the moving position of equinoxes (from γ_0 of the epoch to γ of the date) is marked with an arrow. The dotted segment $q - A$ is the apsidal line which determines the perihelia (q) and aphelia (A). The direction to the ecliptic's pole is \check{C} . The Earth's equator is drawn over the gray terrestrial sphere, and its continuation determines the Sun's declination (δ) with the Sun-Earth radiovector (\mathbf{r}). In addition, the Earth terrestrial pole direction is marked, which help defines the obliquity ϵ . The Earth's true longitude and the longitude of the perihelion, both of the epoch of reference, are also indicated.

Fig. 3: Precessional elements measured with respect to the fiducial J2000.0 epoch. The mean equator of reference (J2000.0) and the mean equa-

tor of the date, are indicated. The nodal point N is the intersection of the two ecliptics: E_o of the reference epoch, and E_t the ecliptic of the date. The general precession in longitude accumulated from J2000.0 is p_A (i.e., the segment from the projection of γ_0 on E_t , to γ point). See the main text for descriptions of other angles.

Fig. 4: The spherical triangle used to find the “true general precession” and obliquity of the date is shown. The Ω and i elements coming from DE431 define the plane of the Earth’s orbit of the date with respect to the reference epoch (J2000.0). See the text for more details.

Fig. 5: Short-term evolution of the Earth’s eccentricity over 13 kyr (one datum per 120 d). The last 500 yr, from 1950, is illustrated in the insert with expanded details.

Fig. 6: Short-term evolution of the Earth’s longitude of the perihelion over 13 kyr (one datum per 120 d). The last 500 yr, from 1950, is illustrated in the insert with expanded details.

Fig. 7: Short-term evolution of the Earth’s climatic precession over 13 kyr (one datum per 120 d). The last 500 yr, from 1950, is illustrated in the insert with expanded details.

Fig. 8: Short-term evolution of the Earth’s obliquity over 13 kyr (one datum per 120 d). The last 500 yr, from 1950, is illustrated in the insert

with expanded details.

Fig. 9: MTM power spectrum of the raw data from the simulated perturbations on Earth's eccentricity by Venus to Saturn over 1 kyr (from 1000 to 2000 AD). The labels mark the main recognized perturbations. P, P2 and P3 refer to perturbations peaks with confidence level less than 95% which are related to planet Mars. One un-labeled peak between P2 and 2V-3E seems to be associated with the 4E-7Ma inequality. The other un-labeled but significant peaks are harmonics of labeled perturbations.

Fig. 10: MTM power spectrum for the short-term eccentricity variations based on the detrended data series after removing a parabolic long-term trend. The basic periodicities identified in Fig. 9 can also be detected here.

Fig. 11: MTM power spectrum of the detrended obliquity time series. The main periodicities are identified (see discussion in the main text). Other periodicities are from harmonics and non-linear mixing of frequencies.

Fig. 12: Daily mean irradiation at 65°N over the indicated calendar interval for equinoxes; i.e., $\lambda_{\odot t} = 0, 180$ deg. The solar constant used was 1366 W m^{-2} .

Fig. 13: The same as Fig. 12 but for solstices; i.e., $\lambda_{\odot t} = 90, 270$ deg. The solar constant used was 1366 W m^{-2} .

Fig. 14: W at July mid-month; i.e., $\lambda_{\odot t} = 120$ deg., for 65°N . The time interval corresponds closest to the one considered in Loutre et al. (1992)'s Fig. 12a. This comparison shows a very good agreement with their results. Solar constant used was 1366 W m^{-2} .

Fig. 15: MTM spectrum of W (over detrended time series) at July mid-month, 65°N . The main periodicities are identified and are described in the main text. At lower latitudes, the periodicities arising from the obliquity signals are weakened.

Fig. 16: Relative difference in W calculation as a continuous $\lambda_{\odot t}$ or using tabulated values at mid-day, for solstices ($\lambda_{\odot t} = 90, 270$ deg.). At these moments, when the Sun is stationary, the errors are small, but they can reach 0.2%.

Fig. 17: The same as Fig. 16 but for equinoxes ($\lambda_{\odot t} = 0, 180$ deg.). The error is larger on average by one order of magnitude (or about 1.2 %) when compared to the errors during solstices.

Fig. 18: Relative difference in the W calculation as a function of $\lambda_{\odot t}$ over the 13 kyr interval we studied (for 65°N). Around the solstice of December, the relative error can reach 5% but drop to the level of less than 0.1% at 270 deg.

Fig. 19: W calculation as a continuous $\lambda_{\odot t}$ (lines) or using tabulated values at mid-day (dots), for $\lambda_{\odot t} = 250$ deg. (for 65°N), from 1000 to 2000 AD. The absolute difference is less than 0.3 W m^{-2} .

Fig. 20: Difference $W - W_0$ in mean daily insolation calculation as a function of $\lambda_{\odot t}$ for the 13 kyr interval we studied (for 65°N). At boreal spring and at the end of the boreal summer, the absolute difference can reach 2.5 W m^{-2} (see the text for more explanation).

Fig. 21: W at July mid-month ($\lambda_{\odot t} = 120$ deg.), for 65°N : this work, DE431-IAU (dashed lines); Laskar et al. (2011a) solution, La2010 (points). The comparison is shown starting at -10 kyr with expanded details of the intercomparison illustrated in the insert. The solar constant used was 1366.0 W m^{-2} .

Fig. 22: W at July mid-month ($\lambda_{\odot t} = 120$ deg.), for 65°N : DE431-IAU solution, continuous values (dashed lines); La2010 data (points) and DE431-IAU solution, with tabulated values (dots). Differences between the continuous and tabulated values can reach $\pm 0.3\%$; i.e., approximately $\pm 1.2 \text{ W m}^{-2}$.

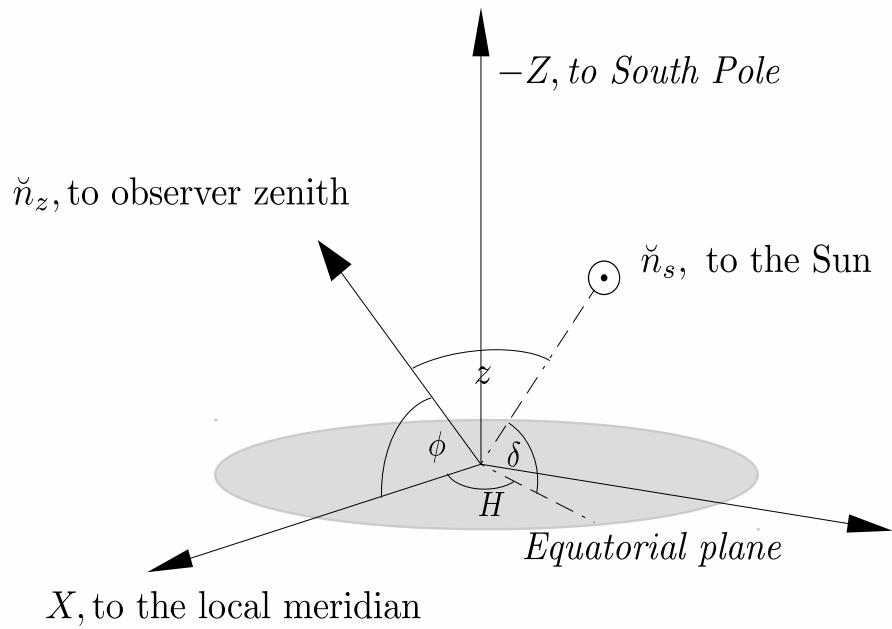


Figure 1: A local fixed geocentric equatorial system (X, Y, Z) is defined; X directed towards the local meridian; minus Z axis directed towards the hemispheric pole (south, here). The minus Y axis points west. The positions of the observer's zenith and the Sun are also indicated.

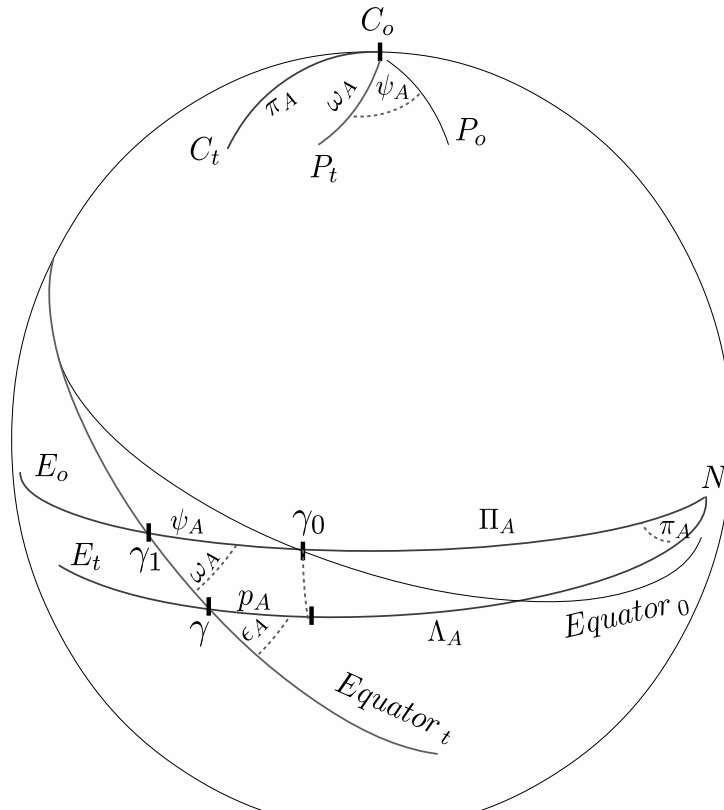


Figure 3: Precessional elements measured with respect to the fiducial J2000.0 epoch. The mean equator of reference (J2000.0) and the mean equator of the date, are indicated. The nodal point N is the intersection of the two ecliptics: E_o of the reference epoch, and E_t the ecliptic of the date. The general precession in longitude accumulated from J2000.0 is p_A (i.e., the segment from the projection of γ_0 on E_t , to γ point). See the main text for descriptions of other angles.

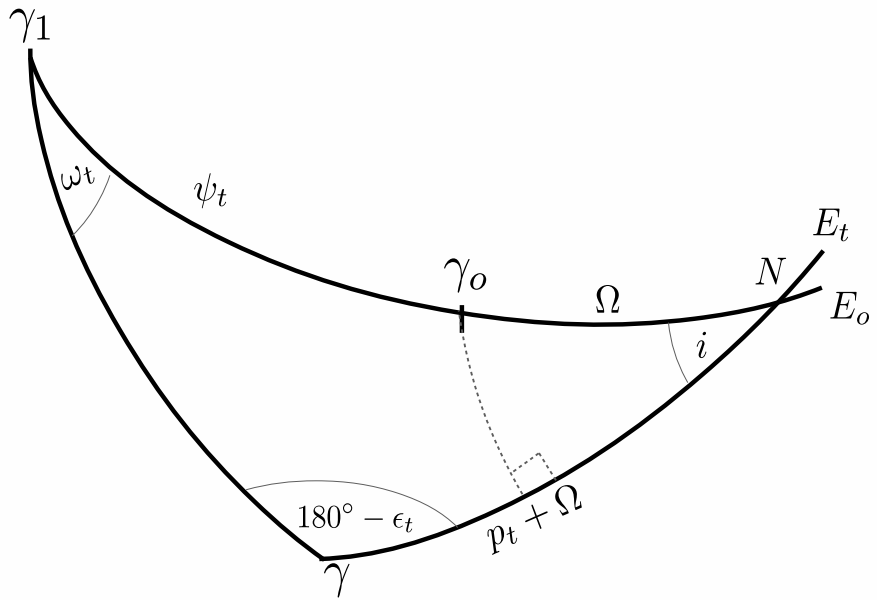


Figure 4: The spherical triangle used to find the “true general precession” and obliquity of the date is shown. The Ω and i elements coming from DE431 define the plane of the Earth’s orbit of the date with respect to the reference epoch (J2000.0). See the text for more details.

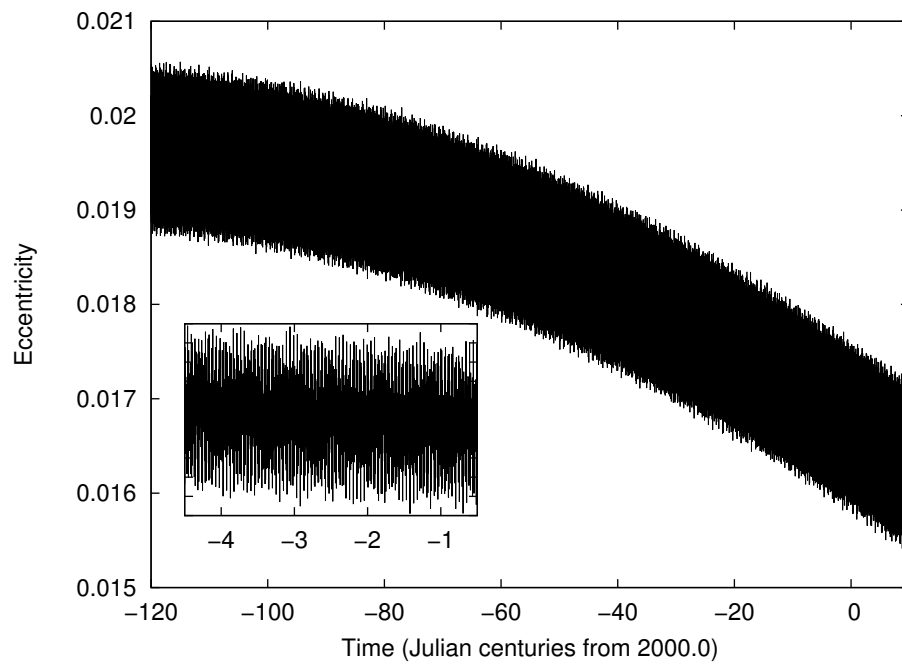


Figure 5: Short-term evolution of the Earth's eccentricity over 13 kyr (one datum per 120 d). The last 500 yr, from 1950, is illustrated in the insert with expanded details.

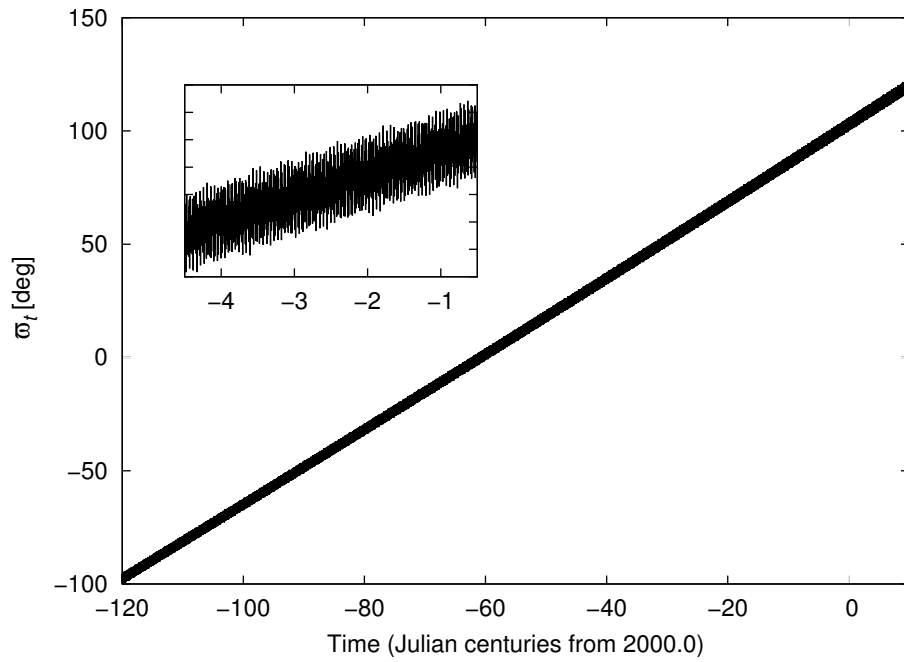


Figure 6: Short-term evolution of the Earth's longitude of the perihelion over 13 kyr (one datum per 120 d). The last 500 yr, from 1950, is illustrated in the insert with expanded details.

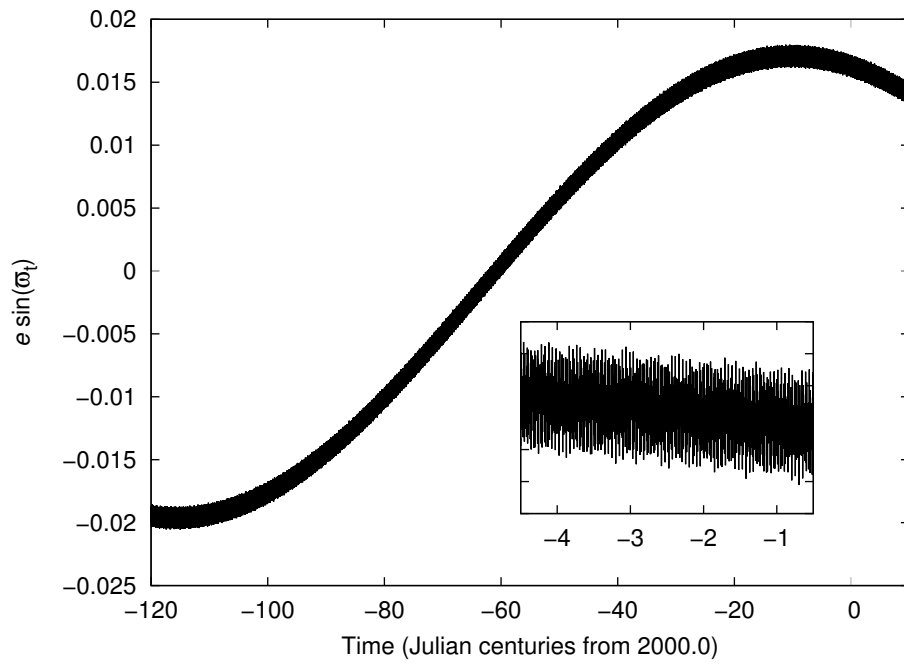


Figure 7: Short-term evolution of the Earth's climatic precession over 13 kyr (one datum per 120 d). The last 500 yr, from 1950, is illustrated in the insert with expanded details.

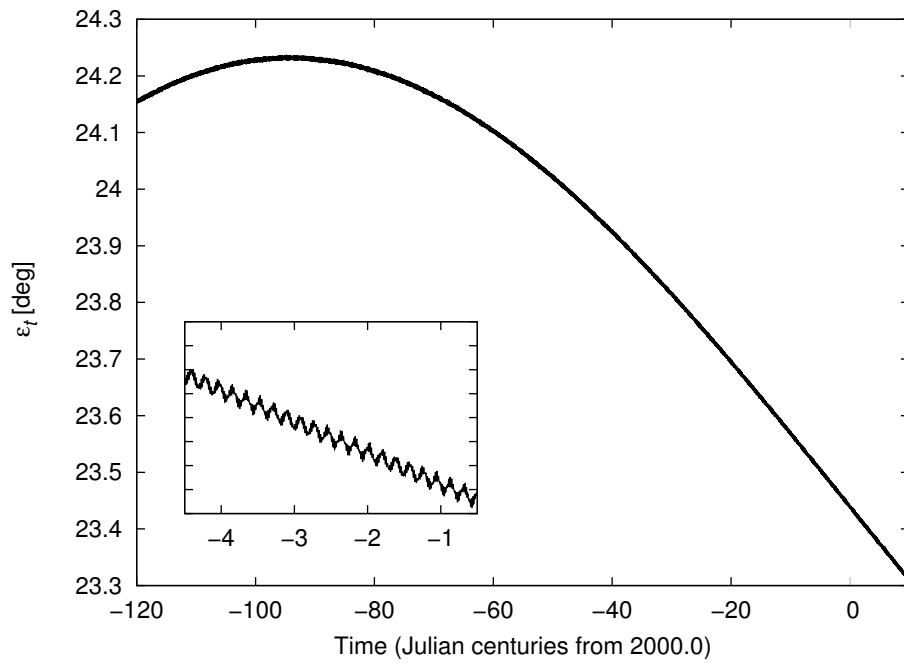


Figure 8: Short-term evolution of the Earth's obliquity over 13 kyr (one datum per 120 d). The last 500 yr, from 1950, is illustrated in the insert with expanded details.

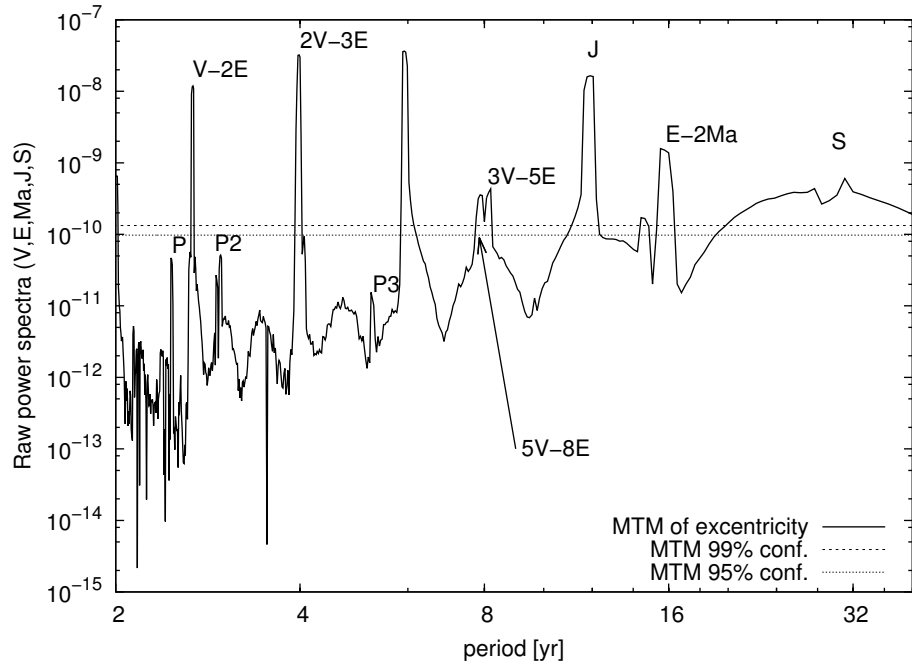


Figure 9: MTM power spectrum of the raw data from the simulated perturbations on Earth's eccentricity by Venus to Saturn over 1 kyr (from 1000 to 2000 AD). The labels mark the main recognized perturbations. P, P2 and P3 refer to perturbations peaks with confidence level less than 95% which are related to planet Mars. One un-labeled peak between P2 and 2V-3E seems to be associated with the 4E-7Ma inequality. The other un-labeled but significant peaks are harmonics of labeled perturbations.

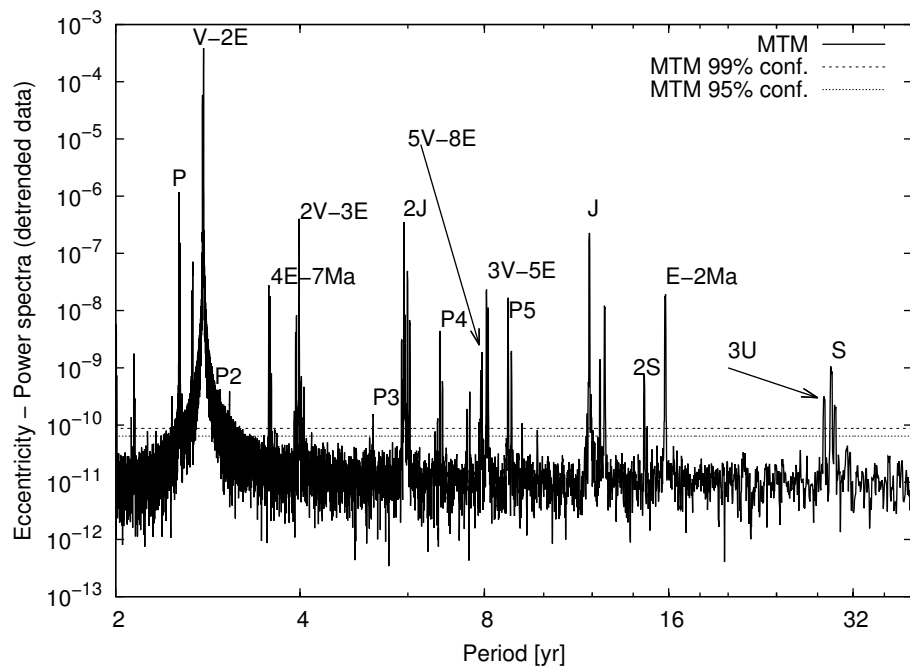


Figure 10: MTM power spectrum for the short-term eccentricity variations based on the detrended data series after removing a parabolic long-term trend. The basic periodicities identified in Fig. 9 can also be detected here.

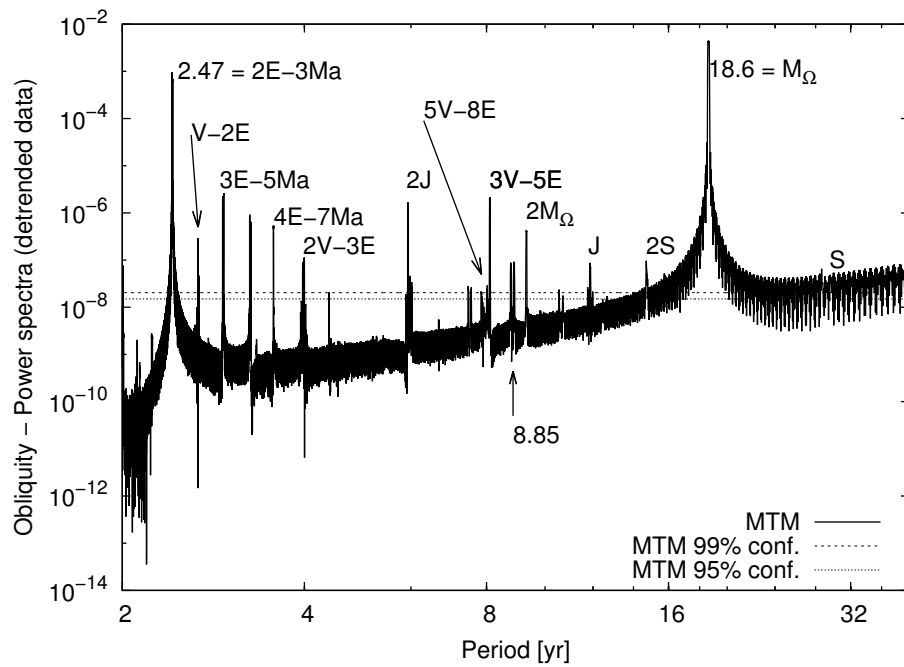


Figure 11: MTM power spectrum of the detrended obliquity time series. The main periodicities are identified (see discussion in the main text). Other periodicities are from harmonics and non-linear mixing of frequencies.

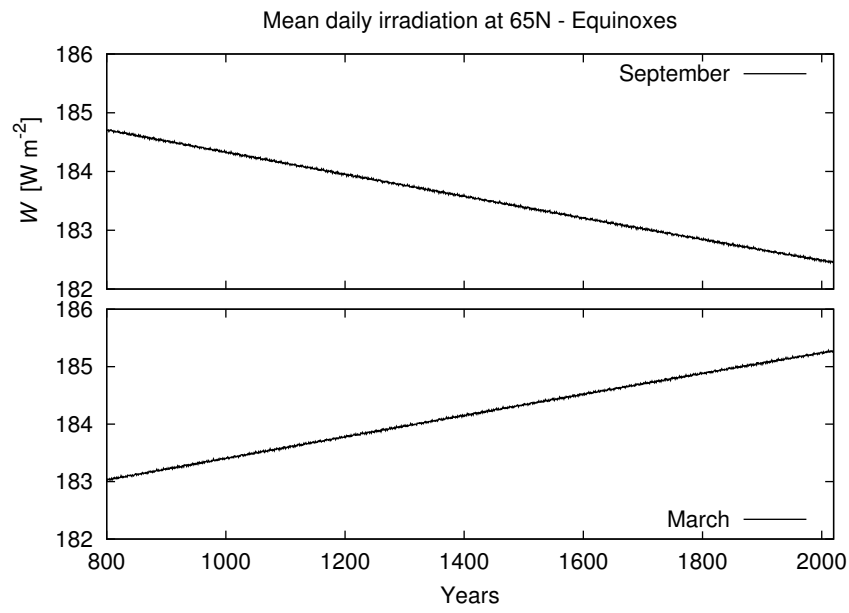


Figure 12: Daily mean irradiation at $65^{\circ}N$ over the indicated calendar interval for equinoxes; i.e., $\lambda_{\odot t} = 0, 180$ deg. The solar constant used was $1366 W m^{-2}$.

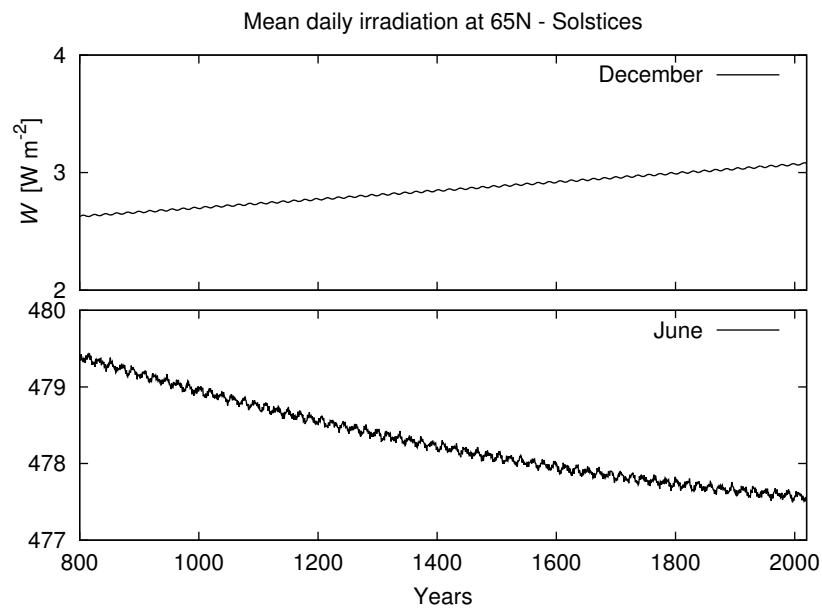


Figure 13: The same as Fig. 12 but for solstices; i.e., $\lambda_{\odot t} = 90, 270$ deg. The solar constant used was 1366 W m^{-2} .

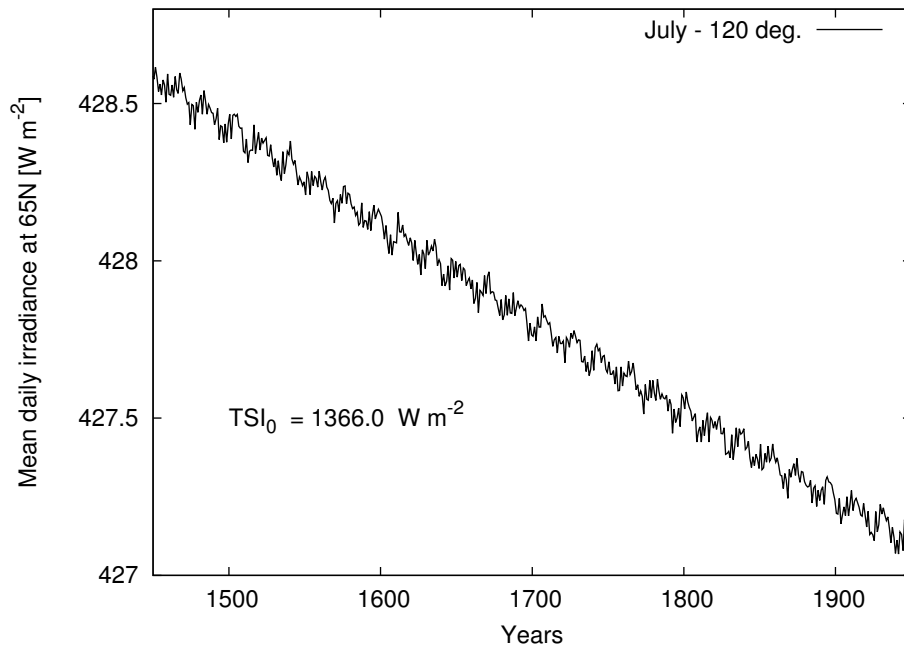


Figure 14: W at July mid-month; i.e., $\lambda_{\odot t} = 120$ deg., for 65°N . The time interval corresponds closest to the one considered in Loutre et al. (1992)'s Fig. 12a. This comparison shows a very good agreement with their results. Solar constant used was 1366 W m^{-2} .

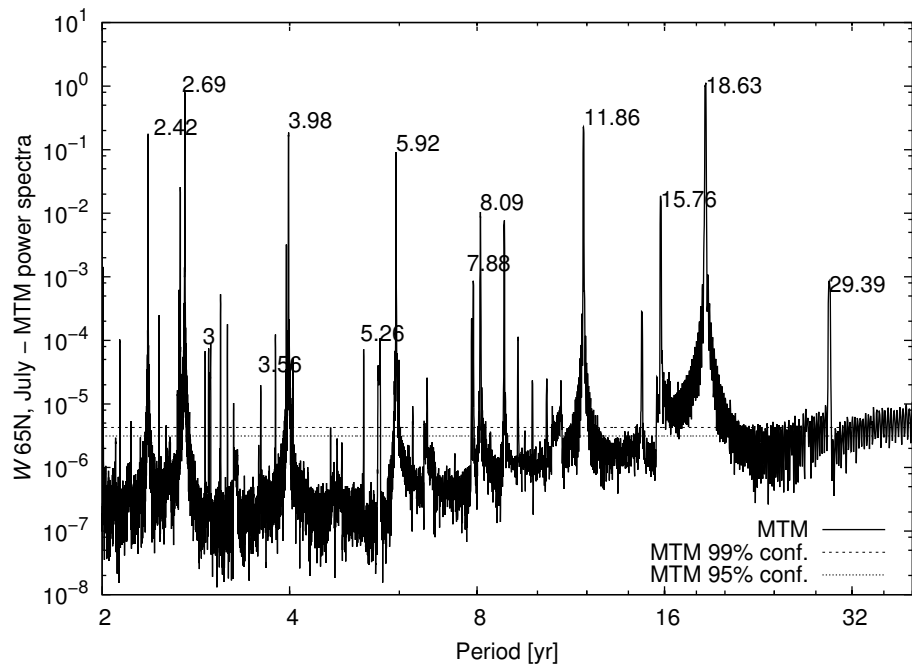


Figure 15: MTM spectrum of W (over detrended time series) at July mid-month, 65°N . The main periodicities are identified and are described in the main text. At lower latitudes, the periodicities arising from the obliquity signals are weakened.

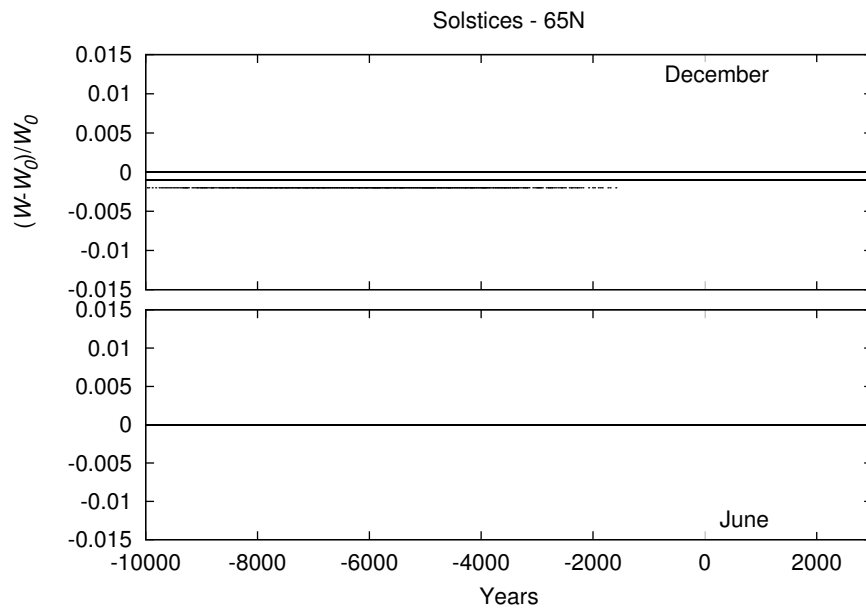


Figure 16: Relative difference in W calculation as a continuous $\lambda_{\odot t}$ or using tabulated values at mid-day, for solstices ($\lambda_{\odot t} = 90, 270$ deg.). At these moments, when the Sun is stationary, the errors are small, but they can reach 0.2%.

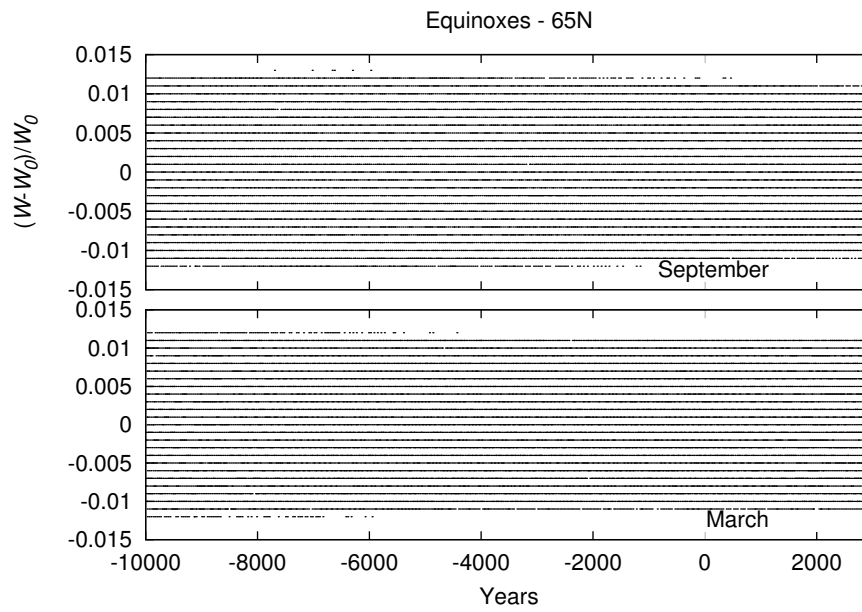


Figure 17: The same as Fig. 16 but for equinoxes ($\lambda_{\odot t} = 0, 180 \text{ deg.}$). The error is larger on average by one order of magnitude (or about 1.2 %) when compared to the errors during solstices.

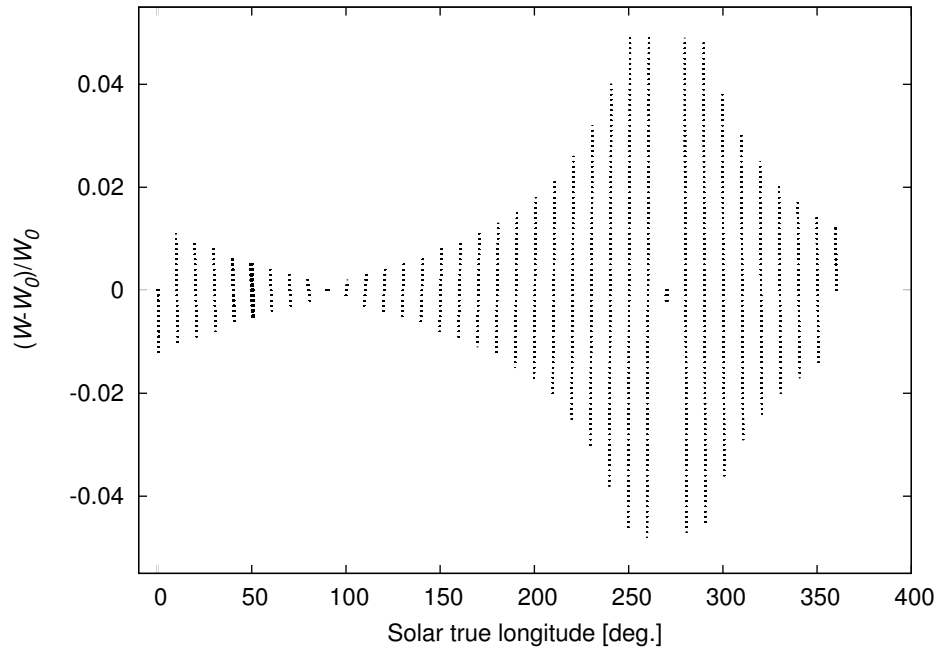


Figure 18: Relative difference in the W calculation as a function of $\lambda_{\odot t}$ over the 13 kyr interval we studied (for 65°N). Around the solstice of December, the relative error can reach 5% but drop to the level of less than 0.1% at 270 deg.

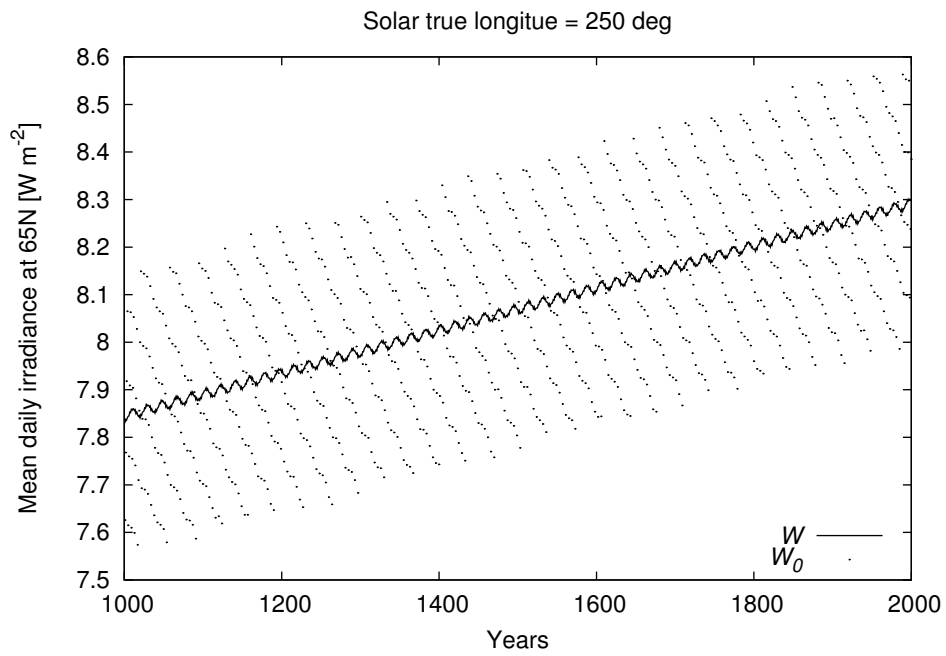


Figure 19: W calculation as a continuous $\lambda_{\odot t}$ (lines) or using tabulated values at mid-day (dots), for $\lambda_{\odot t} = 250$ deg. (for 65°N), from 1000 to 2000 AD. The absolute difference is less than 0.3 W m^{-2} .

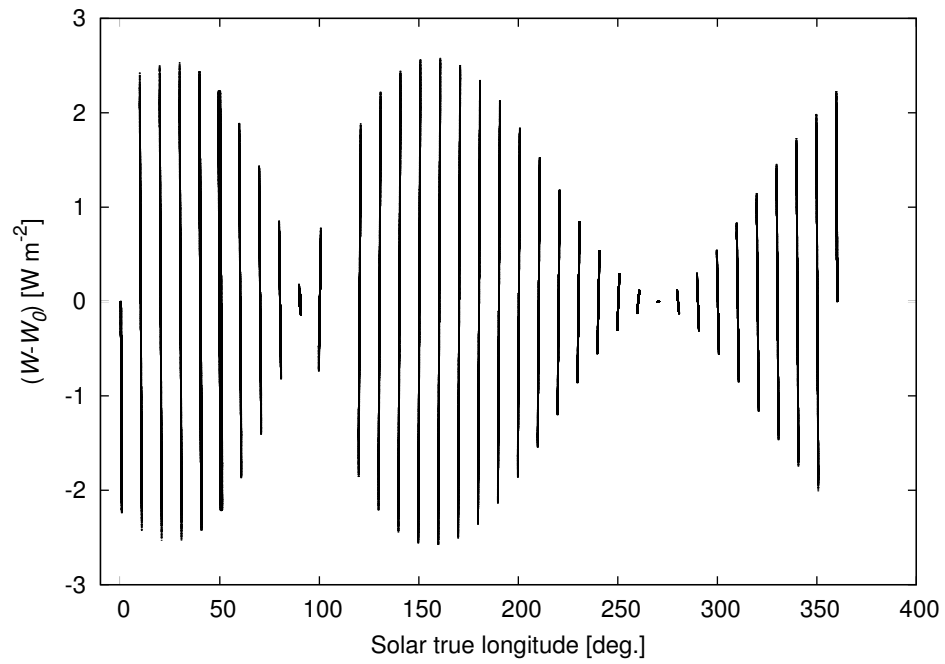


Figure 20: Difference $W - W_0$ in mean daily insolation calculation as a function of $\lambda_{\odot t}$ for the 13 kyr interval we studied (for 65°N). At boreal spring and at the end of the boreal summer, the absolute difference can reach 2.5 W m^{-2} (see the text for more explanation).

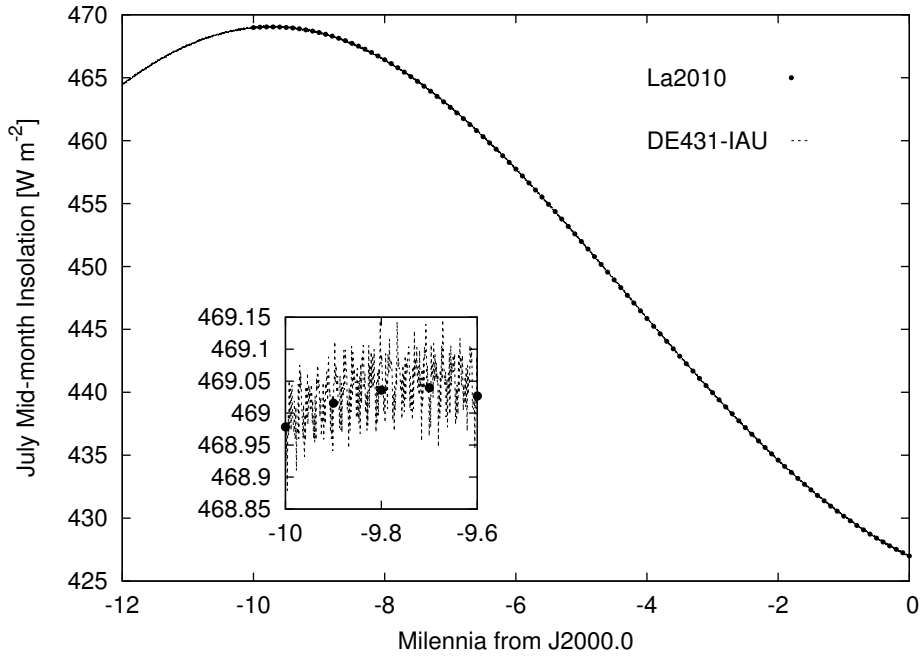


Figure 21: W at July mid-month ($\lambda_{\odot t} = 120$ deg.), for 65°N : this work, DE431-IAU (dashed lines); Laskar et al. (2011a) solution, La2010 (points). The comparison is shown starting at -10 kyr with expanded details of the intercomparison illustrated in the insert. The solar constant used was 1366.0 W m^{-2} .

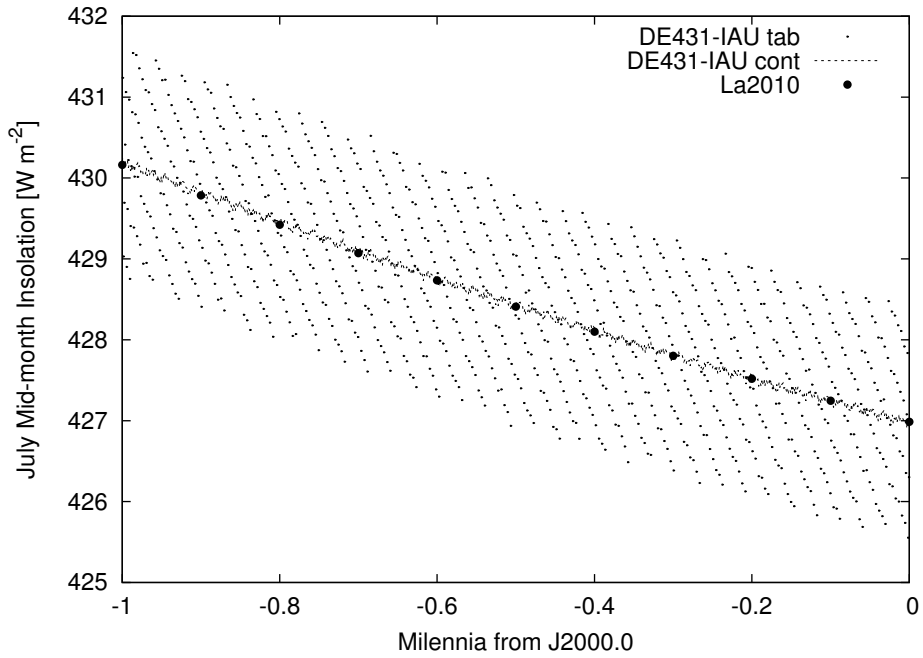


Figure 22: W at July mid-month ($\lambda_{\odot t} = 120$ deg.), for 65°N : DE431-IAU solution, continuous values (dashed lines); La2010 data (points) and DE431-IAU solution, with tabulated values (dots). Differences between the continuous and tabulated values can reach $\pm 0.3\%$; i.e., approximately $\pm 1.2 \text{ W m}^{-2}$.